

A Galerkin least squares approach for photoacoustic tomography*

Johannes Schwab
Sergiy Pereverzyev Jr.
Markus Haltmeier[†]

Department of Mathematics University of Innsbruck
Technikerstrasse 13, A-6020 Innsbruck, Austria

Abstract

The development of fast and accurate image reconstruction algorithms is a central aspect of computed tomography. In this paper we address this issue for photoacoustic computed tomography in circular geometry. We investigate the Galerkin least squares method for that purpose. For approximating the function to be recovered we use subspaces of translation invariant spaces generated by a single function. This includes many systems that have previously been employed in PAT such as generalized Kaiser-Bessel basis functions or the natural pixel basis. By exploiting an isometry property of the forward problem we are able to efficiently set up the Galerkin equation for a wide class of generating functions and devise efficient algorithms for its solution. We establish a convergence analysis and present numerical simulations that demonstrate the efficiency and accuracy of the derived algorithm.

Key words: Photoacoustic imaging, computed tomography, Galerkin least squares method, Kaiser-Bessel functions, Radon transform, least-squares approach.

AMS subject classification: 65R32, 45Q05, 92C55.

1 Introduction

Photoacoustic tomography (PAT) is an emerging non-invasive tomographic imaging modality that allows high resolution imaging with high contrast. Applications are ranging from breast screening in patients to whole body imaging of small animals [4, 45, 27, 58]. The basic principle of PAT is as follows. If a semitransparent sample is illuminated with a short pulse, then parts of the optical energy are absorbed inside the sample (see Figure 1.1). This causes a rapid thermoelastic expansion, which in turns induces an acoustic pressure wave. The

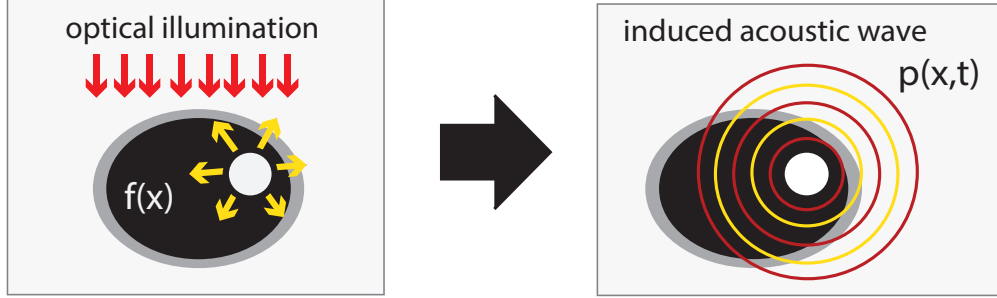


Figure 1.1: BASIC PRINCIPLE OF PAT. Pulsed optical illumination and subsequent thermal expansion induces an acoustic pressure wave. The pressure wave is measured outside of the object and used to obtain an image of the interior.

pressure wave is measured outside of the sample and used for reconstructing an image of the interior.

In this paper we work with the standard model of PAT, where the acoustic pressure $p: \mathbb{R}^d \times (0, \infty) \rightarrow \mathbb{R}$ solves the standard wave equation

$$\begin{cases} \partial_t^2 p(x, t) - \Delta_x p(x, t) = 0, & \text{for } (x, t) \in \mathbb{R}^d \times (0, \infty), \\ p(x, 0) = f(x), & \text{for } x \in \mathbb{R}^d, \\ \partial_t p(x, 0) = 0, & \text{for } x \in \mathbb{R}^d. \end{cases} \quad (1.1)$$

Here d is the spatial dimension, $f: \mathbb{R}^d \rightarrow \mathbb{R}$ the absorbed energy distribution, Δ_x the spatial Laplacian, and ∂_t the derivative with respect to the time variable t . The speed of sound is assumed to be constant and has been rescaled to one. We further suppose that f vanishes outside an open ball $B_R(0) \subseteq \mathbb{R}^d$. The goal of PAT is to recover the function f from measurements of $\mathbf{W}f := p|_{\partial B_R(0) \times (0, \infty)}$. Evaluation of \mathbf{W} is referred to as the direct problem and the problem of reconstructing f from (possibly approximate) knowledge of $\mathbf{W}f$ as the inverse problem of PAT. The cases $d = 3$ and $d = 2$ are of actual relevance in PAT (see [29, 7]).

In the recent years several solution methods for the inverse problem of PAT have been derived. These approaches can be classified in direct methods on the one and iterative (model based) approaches on the other hand. Direct methods are based on explicit solutions for inverting the operator \mathbf{W} that can be implemented numerically. This includes time reversal (see [8, 24, 12, 43, 54]), Fourier domain algorithms (see [1, 20, 31, 46, 53, 59]), and explicit reconstruction formulas of the back-projection type (see [2, 11, 12, 15, 16, 18, 19, 30, 32, 41, 42, 61]). Model based iterative approaches, on the other hand, are based on a discretization of the forward problem together with numerical solution methods for solving the resulting system of linear equations. Existing iterative approaches use interpolation based discretization (see [9, 47, 48, 52, 62]) or approximation using radially symmetric basis functions (see [56, 57]). Recently, also iterative schemes using a continuous domain formulation of the

***Funding:** Authors gratefully acknowledge the support of the Tyrolean Science Fund (TWF).

†Corresponding author, markus.haltmeier@uibk.ac.at.

adjoint have been studied, see [3, 5, 17]. Direct methods are numerically efficient and robust and have similar complexity as numerically evaluating the forward problem. Iterative methods typically are slower since the forward and adjoint problems have to be evaluated repeatedly. However, iterative methods have the advantage of being flexible as one can easily add regularization terms and incorporate measurement characteristics such as finite sampling, finite bandwidth and finite detectors size (see [9, 22, 51, 55, 56, 60]). Additionally, iterative methods tend to be more accurate in the case of noisy data.

1.1 Proposed Galerkin least squares approach

In this paper we develop a Galerkin approach for PAT that combines advantages of direct and model based approaches. Our method comes with a clear convergence theory, sharp error estimates and an efficient implementation. The Galerkin least squares method for $\mathbf{W}f = g$ consists in finding a minimizer of the restricted least squares functional,

$$f_N := \arg \min \{ \|\mathbf{W}h - g\| \mid h \in \mathcal{X}_N \}, \quad (1.2)$$

where \mathcal{X}_N is a finite dimensional reconstruction space and $\|\cdot\|$ an appropriate Hilbert space norm. If $(\varphi_N^k)_{k \in \Lambda_N}$ is a basis of \mathcal{X}_N then $f_N = \sum_{k \in \Lambda_N} c_{N,k} \varphi_N^k$, where $c_N = (c_{N,k})_{k \in \Lambda_N}$ is the unique solution of the Galerkin equation

$$\mathbf{A}_N c_N = (\langle \mathbf{W} \varphi_N^k, g \rangle)_{k \in \Lambda_N} \quad \text{with} \quad \mathbf{A}_N := (\langle \mathbf{W} \varphi_N^k, \mathbf{W} \varphi_N^\ell \rangle)_{k, \ell \in \Lambda_N}. \quad (1.3)$$

We call the matrix \mathbf{A}_N the (discrete) imaging matrix.

In general, both the computation of the imaging matrix as well as the solution of the Galerkin equation can be numerically expensive. In this paper we demonstrate that for the inverse problem of PAT, both issues can be efficiently implemented. These observations are based on the following:

- ISOMETRY PROPERTY. Using the isometry property of [11, 12] one shows that the entries of the system matrix are given by $\frac{R}{2} \langle \varphi_N^k, \varphi_N^\ell \rangle_{L^2}$; see Theorem 2.2.
- SHIFT INVARIANCE. If, additionally, we take the basis functions φ_N^k as translates of a single generating function $\varphi \in L^2(\mathbb{R}^d)$, then $\langle \varphi_N^k, \varphi_N^\ell \rangle_{L^2} = \langle \varphi_N^0, \varphi_N^{k-\ell} \rangle_{L^2}$ for $k, \ell \in \Lambda_N \subseteq \mathbb{Z}^d$.

Consequently only $2^d |\Lambda_N|$ inner products have to be computed in our Galerkin approach opposed to $|\Lambda_N|(|\Lambda_N|+1)/2 = \mathcal{O}(|\Lambda_N|^2)$ inner products required in the general case. Further, the resulting shift invariant structure of the system matrix allows to efficiently solve the Galerkin equation.

Note that shift invariant spaces are frequently employed in computed tomography and include splines spaces, spaces of bandlimited functions, or spaces generated by Kaiser-Bessel functions. In this paper we will especially use Kaiser-Bessel functions which are often considered as the most suitable basis for computed tomography [23, 34, 39, 44]. For the use in PAT they have first been proposed in [56]. We are not aware of existing Galerkin approaches for tomographic image reconstruction exploiting isometry and shift invariance. However, we

anticipate that similar methods can be derived for other tomographic problems, where an isometry property is known (such as X-ray based CT [28, 40]). We further note that our approach has close relations to the method of approximate inverse, which has frequently been applied to computed tomography [21, 35, 36, 37, 49, 50]. Instead of approximating the unknown function using a prescribed reconstruction space, the method of approximate inverse recovers prescribed moments of the unknown and is somehow dual to the Galerkin approach.

1.2 Outline

The rest of this article is organized as follows. In Section 2 we apply the Galerkin least squares method for the inverse problem of PAT. By using the isometry property we derive a simple characterization of the Galerkin equation in Theorem 2.2. We derive a convergence and stability result for the Galerkin least squares method applied to PAT (see Theorem 2.3). In Section 3 we study shift invariant spaces for computed tomography. As the main results in that section we derive an estimate for the L^2 -approximation error using elements from the shift invariant space. In Section 4 we present details for the Galerkin approach using subspaces of shift invariant spaces. In Section 5 we present numerical studies using our Galerkin approach and compare it to related approaches in the literature. The paper concludes with a conclusion and a short outlook in Section 6.

2 Galerkin approach for PAT

Throughout the following, suppose $d \geq 2$, let $B_R(0) := \{x \in \mathbb{R}^d \mid \|x\| < R\}$ denote the open ball with radius R centered at the origin, and let $L_R^2(\mathbb{R}^d) := \{f \in L^2(\mathbb{R}^d) \mid f(x) = 0 \text{ for } x \in \mathbb{R}^d \setminus B_R(0)\}$ denote the Hilbert space of all square integrable functions which vanish outside $B_R(0)$. For two measurable functions $g_1, g_2: \partial B_R(0) \times (0, \infty) \rightarrow \mathbb{R}$ we write

$$\langle g_1, g_2 \rangle_t := \int_{\partial B_R(0)} \int_0^\infty g_1(z, t) g_2(z, t) t \, dt \, ds(z), \quad (2.1)$$

provided that the integral exists. We further denote by \mathcal{Y} the Hilbert space of all functions $g: \partial B_R(0) \times (0, \infty) \rightarrow \mathbb{R}$ with $\|g\|_t^2 := \langle g, g \rangle_t < \infty$.

2.1 PAT and the wave equation

For initial data $f \in C_c^{[d/2]+2}(B_R(0))$ consider the wave equation (1.1). The solution $p: \mathbb{R}^d \times (0, \infty) \rightarrow \mathbb{R}$ of (1.1) restricted to the boundary of $B_R(0)$ is denoted by $\bar{\mathbf{W}}f: \partial B_R(0) \times (0, \infty) \rightarrow \mathbb{R}$. The associated operator is defined by $\bar{\mathbf{W}}: C_c^{[d/2]+2}(B_R(0)) \subseteq L_R^2(\mathbb{R}^d) \rightarrow \mathcal{Y}: f \mapsto \bar{\mathbf{W}}f$

Lemma 2.1 (Isometry and continuous extension of $\bar{\mathbf{W}}$).

(a) For all $f_1, f_2 \in C_c^{[d/2]+2}(B_R(0))$ we have $\langle f_1, f_2 \rangle = \frac{2}{R} \langle \bar{\mathbf{W}}f_1, \bar{\mathbf{W}}f_2 \rangle_t$.

(b) $\bar{\mathbf{W}}$ uniquely extends to a bounded linear operator $\mathbf{W}: L_R^2(\mathbb{R}^d) \rightarrow \mathcal{Y}$.

(c) For all $f_1, f_2 \in L_R^2(\mathbb{R}^d)$ we have $\langle f_1, f_2 \rangle = \frac{2}{R} \langle \mathbf{W}f_1, \mathbf{W}f_2 \rangle_t$.

Proof. (a): See [11, Equation (1.16)] for d even and [12, Equation (1.16)] for d odd. (Note that the isometry identities in [11, 12] are stated for the wave equation with different initial conditions, and therefore at first glance look different from (a).)

(b), (c): Item (a) implies that \mathbf{W} is bounded with respect to the norms of $L_R^2(\mathbb{R}^d)$ and \mathcal{Y} and defined on a dense subspace of $L_R^2(\mathbb{R}^d)$. Consequently it uniquely extends to a bounded operator $\mathbf{W}: L_R^2(\mathbb{R}^d) \rightarrow \mathcal{Y}$. The continuity of the inner product finally shows the isometry property on $L_R^2(\mathbb{R}^d)$. \square

We call \mathbf{W} the acoustic forward operator. PAT is concerned with the inverse problem of estimating f from potentially noisy and approximate knowledge of $\mathbf{W}f$. In this paper we use the Galerkin least squares method for that purpose.

2.2 Application of the Galerkin method

Let $(\mathcal{X}_N)_{N \in \mathbb{N}}$ and $(\mathcal{Y}_N)_{N \in \mathbb{N}}$ be families of subspaces of $L_R^2(\mathbb{R}^d)$ and \mathcal{Y} , respectively, with $\dim \mathcal{X}_N = \dim \mathcal{Y}_N < \infty$. Further let \mathbf{Q}_N denote the orthogonal projection on \mathcal{Y}_N and suppose $g \in \mathcal{Y}$. The Galerkin method for solving $\mathbf{W}f = g$ defines the approximate solution $f_N \in \mathcal{X}_N$ as the solution of

$$\mathbf{Q}_N \mathbf{W}f_N = \mathbf{Q}_N g. \quad (2.2)$$

In this paper we consider the special case where $\mathcal{Y}_N = \mathbf{W}\mathcal{X}_N$, in which case the solution of (2.2) is referred to as *Galerkin least squares method*. The name comes from the fact that in this case the Galerkin solution can be uniquely characterized as the minimizer of the least squares functional over \mathcal{X}_N ,

$$\Phi_N(f_N) := \frac{1}{2} \|\mathbf{W}f_N - g\|_t^2 \rightarrow \min_{f_N \in \mathcal{X}_N}. \quad (2.3)$$

Because Φ_N is a quadratic functional on a finite dimensional space and \mathbf{W} is injective, (2.3) possesses a unique solution. Together with the isometry property we obtain the following characterizations of the least squares Galerkin method for PAT.

Theorem 2.2 (Characterizations of the Galerkin least squares method). *For $g \in \mathcal{Y}$ and $f_N \in \mathcal{X}_N$ the following are equivalent:*

- (1) $\mathbf{Q}_N \mathbf{W}f_N = \mathbf{Q}_N g$;
- (2) f_N minimizes the least squares functional (2.3);
- (3) For an arbitrary basis $(\varphi_N^k)_{k \in \Lambda_N}$ of \mathcal{X}_N , we have

$$\mathbf{A}_N c_N = d_N \quad (2.4)$$

where

- $c_N := (c_{N,k})_k$ with $f_N = \sum_{k \in \Lambda_N} c_{N,k} \varphi_N^k$;
- $d_N := (\langle \mathbf{W} \varphi_N^k, g \rangle_t)_{k \in \Lambda_N}$;
- $\mathbf{A}_N := (\frac{R}{2} \langle \varphi_N^k, \varphi_N^\ell \rangle_{L^2})_{k, \ell \in \Lambda_N}$.

Proof. The equivalence of (1) and (2) is a standard result for the Galerkin squares method (see, for example, [26]). Another standard characterization shows the equivalence of (1) and (3) with the system matrix $\mathbf{A}_N = (\langle \mathbf{W} \varphi_N^k, \mathbf{W} \varphi_N^\ell \rangle_t)_{k, \ell \in \Lambda_N}$. Now, the isometry property given in Lemma 2.1 shows $\langle \mathbf{W} \varphi_N^k, \mathbf{W} \varphi_N^\ell \rangle_t = \frac{R}{2} \langle \varphi_N^k, \varphi_N^\ell \rangle_{L^2}$ and concludes the proof. \square

In general, evaluating all matrix entries $\langle \mathbf{W} \varphi_N^k, \mathbf{W} \varphi_N^\ell \rangle_t$ can be difficult. For many basis functions an explicit expression for $\mathbf{W} \varphi_N^k$ is not available including the natural pixel basis, spaces defined by linear interpolation, or spline spaces. Hence $\mathbf{W} \varphi_N^k$ has to be evaluated numerically which is time consuming and introduces additional errors. Even if $\mathbf{W} \varphi_N^k$ is given explicitly, then the inner products $\langle \mathbf{W} \varphi_N^k, \mathbf{W} \varphi_N^\ell \rangle_{L^2}$ have to be computed numerically and stored. For large N this can be problematic and time consuming. In contrast, by using the isometry property in our approach we only have to compute the inner products $\langle \varphi_N^k, \varphi_N^\ell \rangle$. Further, in computed tomography it is common to take φ_N^k as translates of a single function φ_N^0 . In such a situation the inner products satisfy $\langle \varphi_N^k, \varphi_N^\ell \rangle = \langle \varphi_N^0, \varphi_N^{\ell-k} \rangle$ and therefore only a small fraction of all inner products actually have to be computed.

2.3 Convergence and stability analysis

As another consequence of the isometry property we derive linear error estimates for the Galerkin approach to PAT. We consider noisy data where the data $g^\delta \in \mathcal{Y}$ is known to satisfy

$$\|\mathbf{W} f^0 - g^\delta\| \leq \delta, \quad (2.5)$$

for some noise level $\delta \geq 0$ and unknown $f^0 \in L_R^2(\mathbb{R}^d)$. For noisy data we define the Galerkin least squares solution by

$$f_N^\delta = \arg \min \{ \|\mathbf{W} h - g^\delta\|_t \mid h \in \mathcal{X}_N \} . \quad (2.6)$$

We then have the following convergence and stability result.

Theorem 2.3 (Convergence and stability of the Galerkin method for PAT). *Let $f^0 \in L_R^2(\mathbb{R}^d)$, $g^\delta \in \mathcal{Y}$, $\delta \geq 0$ satisfy (2.5) and let f_N^δ be defined by (2.6). Then, the following error estimate for the Galerkin method holds:*

$$\|f_N^\delta - f^0\| \leq \min\{\|h - f^0\| \mid h \in \mathcal{X}_N\} + \sqrt{\frac{2}{R}} \delta. \quad (2.7)$$

Proof. We start with the noise free case $\delta = 0$. The definition of f_N^δ and the isometry property of \mathbf{W} yield

$$\begin{aligned} f_N^0 &= \arg \min \{ \|\mathbf{W} h - g^0\|_t \mid h \in \mathcal{X}_N \} \\ &= \arg \min \{ \|\mathbf{W} h - \mathbf{W} f^0\|_t \mid h \in \mathcal{X}_N \} \end{aligned}$$

$$= \arg \min \{ \|h - f^0\| \mid h \in \mathcal{X}_N \}$$

This shows $f_N^0 = \mathbf{P}_{\mathcal{X}_N} f^0$ and yields (2.7) for $\delta = 0$. Here and below we use \mathbf{P}_V to denote the orthogonal projection on a closed subspace $V \subseteq L_R^2(\mathbb{R}^d)$.

Now consider the case of arbitrary δ , with $g^\delta = \mathbf{W}f^0 + e^\delta$ where $e^\delta \in \mathcal{Y}$ satisfies $\|e^\delta\| \leq \delta$. Because $\text{Ran}(\mathbf{W})$ is closed we can write

$$g^\delta = (\mathbf{W}f^0 + \mathbf{P}_{\text{Ran}(\mathbf{W})}(e^\delta)) + \mathbf{P}_{\text{Ran}(\mathbf{W})^\perp}(e^\delta) =: \mathbf{W}f^\delta + \mathbf{P}_{\text{Ran}(\mathbf{W})^\perp}(e^\delta).$$

Following the case $\delta = 0$ and using that $\mathbf{P}_{\text{Ran}(\mathbf{W})^\perp}(e^\delta) \perp \text{Ran}(\mathbf{W})$ one verifies that $f_N^\delta = \mathbf{P}_{\mathcal{X}_N} f^\delta$. Therefore, by the triangle inequality and the isometry property of \mathbf{W} we obtain

$$\begin{aligned} \|f_N^\delta - f^0\| &\leq \|f_N^\delta - f_N^0\| + \|f_N^0 - f^0\| \\ &= \|\mathbf{P}_{\mathcal{X}_N}(f^\delta - f^0)\| + \min\{\|h - f^0\| \mid h \in \mathcal{X}_N\} \\ &\leq \sqrt{\frac{2}{R}} \|\mathbf{W}f^\delta - \mathbf{W}f^0\|_t + \min\{\|h - f^0\| \mid h \in \mathcal{X}_N\}. \end{aligned}$$

Together with $\|\mathbf{W}f^\delta - \mathbf{W}f^0\|_t = \|\mathbf{P}_{\text{Ran}(\mathbf{W})}(e^\delta)\|_t \leq \delta$ this concludes the proof. \square

The error estimate in Theorem 2.3 depends on two terms: the first term depends on the approximation properties of the space \mathcal{X}_N and the second term on the noise level δ . As easily verified both terms are optimal and cannot be improved. The second term shows stability of our Galerkin least squares approach. Under the reasonable assumption that the spaces \mathcal{X}_N satisfy the denseness property

$$\forall f \in L_R^2(\mathbb{R}^d): \quad \lim_{N \rightarrow \infty} \min\{\|h - f\| \mid h \in \mathcal{X}_N\} = 0,$$

the derived error estimate further implies convergence of the Galerkin approach.

3 Shift invariant spaces in computed tomography

In many tomographic and signal processing applications, natural spaces for approximating the underlying function are subspaces of shift invariant spaces. In this paper we consider spaces $\mathcal{V}_{T,s,\varphi}$ that are generated by translated and scaled versions of a single function $\varphi \in L^2(\mathbb{R}^d)$,

$$\mathcal{V}_{T,s,\varphi} := \overline{\text{span}(\{\varphi_{T,s}^k \mid k \in \mathbb{Z}^d\})} \subseteq L^2(\mathbb{R}^d). \quad (3.1)$$

Here span denotes the linear hull, \overline{X} stands for the closure with respect to $\|\cdot\|_{L^2}$ of a set X , and

$$\varphi_{T,s}^k(x) := \frac{1}{T^{d/2}} \varphi\left(\frac{x}{T} - sk\right) \quad \text{for } T, s > 0 \text{ and } k \in \mathbb{Z}^d. \quad (3.2)$$

We have chosen the normalization of the generating functions $\varphi_{T,s}^k$ in such a way that $\|\varphi_{T,s}^k\|_{L^2} = \|\varphi\|_{L^2}$ for all T, s, k . In this section we derive conditions such that any L^2 function can be approximated by elements in $\mathcal{V}_{T,s,\varphi}$. Further, we present examples of generating functions that are relevant for (photoacoustic) computed tomography.

Any tomographic reconstruction method uses, either explicitly or implicitly, a particular discrete reconstruction space. This is obvious for any iterative procedure as it requires a finite dimensional representation of the forward operator that can be evaluated numerically. However, also direct methods use an underlying discrete image space. For example, standard filtered backprojection algorithms usually reconstruct samples of a bandlimited approximation of the unknown function. In such a situation, the underlying discrete signal space consists of bandlimited functions. In this paper we allow more general shift invariant spaces.

The following properties of the generating function and the spaces $\mathcal{V}_{T,s,\varphi}$ have been reported desirable for tomographic applications (see [44, 56]):

(V1) φ has “small” spatial support;

(V2) φ is rotationally invariant;

(V3) $(\varphi_{T,s}^k)_{k \in \mathbb{Z}^d}$ is a Riesz basis of $\mathcal{V}_{T,s,\varphi}$;

(V4) φ satisfies the so called partition of unity property.

Conditions (V1) and (V2) are desirable from a computational point of view and often help to derive efficient reconstruction algorithms. The properties (V3) and (V4) are of more fundamental nature as these conditions imply that any L^2 function can be approximated arbitrarily well by elements in $\mathcal{V}_{T,s,\varphi}$ as $T \rightarrow 0$ (with s kept fixed; the so called stationary case). In [44] it has been pointed out that the properties (V1)-(V4) cannot be simultaneously fulfilled. This implies that for taking s independent of T , the spaces $\mathcal{V}_{T,s,\varphi}$ have a limited approximation capability in the sense that for a typical function f , the approximation error $\min_{u \in \mathcal{V}_{T,s,\varphi}} \|f - u\|_{L^2}^2$ does not converge to zero as $T \rightarrow 0$ and s is kept fixed.

Despite these negative results, radially symmetric basis functions are of great popularity in computed tomography (see for example, [23, 33, 34, 39, 44, 57, 56]). In this paper we therefore propose to also allow the shift parameter s to be variable. Under reasonable assumptions we show that the approximation error converges to zero for $s \rightarrow 0$. This convergence in particular holds for radially symmetric generating functions having some decay in the Fourier space, including generalized Kaiser-Bessel functions which are the most popular choice in tomographic image reconstruction.

3.1 Riesz bases of shift invariant spaces

Recall that the family $(\varphi_{T,s}^k)_{k \in \mathbb{Z}^d}$ is called a Riesz basis of $\mathcal{V}_{T,s,\varphi}$ if there exist $A, B > 0$ such that

$$\forall c \in \ell^2(\mathbb{Z}^d): \quad A \|c\|_{\ell^2}^2 \leq \left\| \sum_{k \in \mathbb{Z}^d} c_k \varphi_{T,s}^k \right\|_{L^2}^2 \leq B \|c\|_{\ell^2}^2, \quad (3.3)$$

where $\|c\|_{\ell^2}^2 := \sum_{k \in \mathbb{Z}^d} |c_k|^2$ is the squared ℓ^2 -norm of $c = (c_k)_{k \in \mathbb{Z}^d}$. A Riesz basis of $\mathcal{V}_{T,s,\varphi}$ can equivalently be defined as a linear independent family of frames and the constants A and B are the lower and upper frame bounds of $(\varphi_{T,s}^k)_{k \in \mathbb{Z}^d}$, respectively. In the following we write $\hat{\varphi}$ for the d -dimensional Fourier transform defined by $\hat{\varphi}(\xi) := (2\pi)^{-d/2} \int_{\mathbb{R}^d} \varphi(x) e^{-i\xi \cdot x} dx$ for $\varphi \in L^2(\mathbb{R}^d) \cap L^1(\mathbb{R}^d)$ and extended to $L^2(\mathbb{R}^d)$ by continuity.

The following two Lemmas are well known in the case that $d = T = 1$ (see [38, Theorem 3.4]). Due to page limitations and because the general case is shown analogously, the proofs of the Lemmas are omitted.

Lemma 3.1 (Riesz basis property). *The family $(\varphi_{T,s}^k)_{k \in \mathbb{Z}^d}$ is a Riesz basis of $\mathcal{V}_{T,s,\varphi}$ with frame bounds A and B , if and only if*

$$\frac{A}{(2\pi)^d} \leq \frac{1}{s^d} \sum_{k \in \mathbb{Z}^d} |\hat{\varphi}(\xi + \frac{2\pi}{s}k)|^2 \leq \frac{B}{(2\pi)^d} \quad \text{for a.e. } \xi \in [0, \frac{2\pi}{s}]^d. \quad (3.4)$$

Proof. Follows the lines of [38, Theorem 3.4]. □

The following Lemma implies that for any Riesz basis $(\varphi_{T,s}^k)_{k \in \mathbb{Z}^d}$ one can construct an orthonormal basis of $\mathcal{V}_{T,s,\varphi}$ that is again generated by translated and scaled versions $\theta_{T,s}^k(x) := T^{-d/2}\theta(x/T - sk)$ of a single function $\theta \in L^2(\mathbb{R}^d)$.

Lemma 3.2 (Orthonormalization). *Let $(\varphi_{T,s}^k)_{k \in \mathbb{Z}^d}$ be a Riesz basis of $\mathcal{V}_{T,s,\varphi}$.*

(a) $(\varphi_{T,s}^k)_{k \in \mathbb{Z}^d}$ orthonormal $\iff \sum_{k \in \mathbb{Z}^d} |\hat{\varphi}(\xi + \frac{2\pi}{s}k)|^2 = \frac{s^d}{(2\pi)^d}$ for a.e. $\xi \in \mathbb{R}^d$.

(b) $(\theta_{T,s}^k)_{k \in \mathbb{Z}^d}$ is an orthonormal basis of $\mathcal{V}_{T,s,\varphi}$, where $\theta \in L^2(\mathbb{R}^d)$ is defined by

$$\hat{\theta}(\xi) = \frac{s^{d/2}\hat{\varphi}(\xi)}{(2\pi)^{d/2}\sqrt{\sum_{k \in \mathbb{Z}^d} |\hat{\varphi}(\xi + \frac{2\pi}{s}k)|^2}}. \quad (3.5)$$

Proof. Follows the lines of [38, Theorem 3.4]. □

According to Lemma 3.2, for theoretical purposes one may assume that the considered basis of $\mathcal{V}_{T,s,\varphi}$ is already orthogonal. From a practical point of view, however, it may be more convenient to work with the original non-orthogonal basis. The function φ may have additional properties such as small support or radial symmetry which may not be the case for θ . Also it may not be the case that θ is known analytically.

3.2 The L^2 -approximation error

We now investigate the L^2 -approximation error in shift invariant spaces,

$$\forall f \in L^2(\mathbb{R}^d): \quad \min_{u \in \mathcal{V}_{T,s,\varphi}} \|f - u\|_{L^2} = \|f - \mathbf{P}_{T,s}f\|_{L^2}, \quad (3.6)$$

as well as its asymptotic properties. Here and in the following $\mathbf{P}_{T,s}: L^2(\mathbb{R}^d) \rightarrow \mathcal{V}_{T,s,\varphi}$ denotes the orthogonal projection on $\mathcal{V}_{T,s,\varphi}$. It is given by $\mathbf{P}_{T,s}f = \sum_{\lambda \in \Lambda} \langle f, e_\lambda \rangle e_\lambda$, where $(e_\lambda)_{\lambda \in \Lambda}$ is any orthogonal basis of $\mathcal{V}_{T,s,\varphi}$. For the stationary case $s = 1$, the following Theorem has been obtained in [6].

Theorem 3.3 (The L^2 -approximation error). Let $(\varphi_{T,s}^k)_{k \in \mathbb{Z}^d}$ be a Riesz basis of $\mathcal{V}_{T,s,\varphi}$ and define

$$\mathcal{E}_\varphi(s, T\xi) := 1 - \frac{|\hat{\varphi}(T\xi)|^2}{\sum_{k \in \mathbb{Z}^d} |\hat{\varphi}(T\xi + 2k\pi/s)|^2} \quad \text{for } \xi \in \mathbb{R}^d \text{ and } T, s > 0. \quad (3.7)$$

Then, for every $f \in W_2^r(\mathbb{R}^d)$ with $r > d/2$ we have

$$\|\mathbf{P}_{T,s}f - f\|_{L^2} = \left[\int_{[-\frac{\pi}{Ts}, \frac{\pi}{Ts}]^d} |\hat{f}(\xi)|^2 \mathcal{E}_\varphi(s, T\xi) d\xi \right]^{\frac{1}{2}} + \mathcal{R}_\varphi(f, Ts), \quad (3.8)$$

where the remainder can be estimated as

$$\mathcal{R}_\varphi(f, Ts) \leq \|f\|_{W_2^r} \left(\frac{Ts}{\pi} \right)^r \sqrt{\sum_{n \in \mathbb{Z}^d \setminus \{0\}} \frac{1}{\|n\|^{2r}}} \quad \text{for } T, s > 0. \quad (3.9)$$

Proof. Let $(\theta_{T,s}^k)_{k \in \mathbb{Z}^d}$ denote the orthonormal basis of the space $\mathcal{V}_{T,s,\varphi}$ as constructed in Lemma 3.2. Further, for every $n \in \mathbb{Z}^d$ define $Q_n := \frac{2\pi}{Ts}n + [-\frac{\pi}{Ts}, \frac{\pi}{Ts}]^d$ and define functions $f_n \in L^2(\mathbb{R}^d)$ by its Fourier representation

$$\hat{f}_n(\xi) = \begin{cases} \hat{f}(\xi) & \text{if } \xi \in Q_n, \\ 0 & \text{if } \xi \notin Q_n. \end{cases}$$

Then we have $f = \sum_{n \in \mathbb{Z}^d} f_n$ and $\mathbf{P}_{T,s}f - f = \sum_{n \in \mathbb{Z}^d} \mathbf{P}_{T,s}f_n - f_n$.

Now for every $n \in \mathbb{Z}^d$, we investigate the approximation error $\|\mathbf{P}_{T,s}f_n - f_n\|^2$. We have $\|\mathbf{P}_{T,s}f_n - f_n\|^2 = \|f_n\|^2 - \sum_{k \in \mathbb{Z}^d} |\langle f_n, \theta_{T,s}^k \rangle|^2$. Further,

$$\begin{aligned} \langle f_n, \theta_{T,s}^k \rangle &= \langle \hat{f}_n, \hat{\theta}_{T,s}^k \rangle \\ &= T^{d/2} \int_{Q_n} \hat{f}_n(\xi) \overline{\hat{\theta}(T\xi)} e^{-iT_s \xi \cdot k} d\xi \\ &= T^{d/2} \int_{[-\frac{\pi}{Ts}, \frac{\pi}{Ts}]^d} \hat{f}_n(\xi - 2\pi n/(Ts)) \overline{\hat{\theta}(T(\xi - 2\pi n/(Ts)))} e^{iT_s(\xi - 2\pi n/(Ts)) \cdot k} d\xi \\ &= T^{d/2} \int_{[-\frac{\pi}{Ts}, \frac{\pi}{Ts}]^d} \hat{f}_n(\xi - 2\pi n/(Ts)) \overline{\hat{\theta}(T(\xi - 2\pi n/(Ts)))} e^{iT_s \xi \cdot k} d\xi \\ &= T^{d/2} \hat{d}_{n,-k}, \end{aligned}$$

where $\hat{d}_{n,k}$ is the k -th Fourier-coefficient of the $2\pi/(Ts)$ -periodization of the function $\xi \mapsto \hat{f}_n(\xi - 2\pi n/(Ts)) \overline{\hat{\theta}(T(\xi - 2\pi n/(Ts)))}$. Due to Parseval's identity we have

$$\begin{aligned} \sum_{k \in \mathbb{Z}^d} |\langle f_n, \theta_{T,s}^k \rangle|^2 &= T^d \sum_{k \in \mathbb{Z}^d} |\hat{d}_{n,k}|^2 \end{aligned}$$

$$\begin{aligned}
&= T^d \frac{(2\pi)^d}{(sT)^d} \int_{Q_n} |\hat{f}_n(\xi)|^2 |\hat{\theta}(T\xi)|^2 d\xi \\
&= \int_{Q_n} |\hat{f}_n(\xi)|^2 \frac{|\hat{\varphi}(T\xi)|^2}{\sum_{k \in \mathbb{Z}^d} |\hat{\varphi}(T\xi + 2k\pi/s)|^2} d\xi.
\end{aligned}$$

Therefore we obtain

$$\begin{aligned}
\|\mathbf{P}_{T,s}f_n - f_n\|^2 &= \int_{Q_n} |\hat{f}_n(\xi)|^2 \left(1 - \frac{|\hat{\varphi}(T\xi)|^2}{\sum_{k \in \mathbb{Z}^d} |\hat{\varphi}(T\xi + 2k\pi/s)|^2}\right) d\xi \\
&= \int_{Q_n} |\hat{f}_n(\xi)|^2 \mathcal{E}_\varphi(s, T\xi) d\xi.
\end{aligned}$$

Next notice that for $n \in \mathbb{Z}^d \setminus \{0\}$ and $\xi \in Q_n \subseteq \mathbb{R}^d$ we have $\|\xi\| \geq \frac{\pi}{Ts} \|n\|$. Therefore we can estimate

$$\|\mathbf{P}_{T,s}f_n - f_n\| \leq \left(\frac{Ts}{\pi}\right)^r \left(\frac{1}{\|n\|}\right)^r \left(\int_{Q_n} \|\xi\|^{2r} |\hat{f}_n(\xi)|^2 \mathcal{E}_\varphi(s, T\xi) d\xi\right)^{\frac{1}{2}}.$$

Together with the triangle inequality and the Cauchy-Schwarz inequality for sums we obtain

$$\begin{aligned}
&\|\mathbf{P}_{T,s}f - f\| \\
&\leq \sum_{n \in \mathbb{Z}^d} \|\mathbf{P}_{T,s}f_n - f_n\| \\
&\leq \left(\int_{Q_0} |\hat{f}(\xi)|^2 \mathcal{E}_\varphi(s, T\xi) d\xi\right)^{\frac{1}{2}} + \left(\frac{Ts}{\pi}\right)^r \sum_{n \neq 0} \frac{1}{\|n\|^r} \left(\int_{Q_n} \|\xi\|^{2r} |\hat{f}_n(\xi)|^2 d\xi\right)^{\frac{1}{2}} \\
&\leq \left(\int_{Q_0} |\hat{f}(\xi)|^2 \mathcal{E}_\varphi(s, T\xi) d\xi\right)^{\frac{1}{2}} + \left(\frac{Ts}{\pi}\right)^r \left(\sum_{n \neq 0} \frac{1}{\|n\|^{2r}}\right)^{\frac{1}{2}} \left(\int_{\mathbb{R}^d \setminus Q_0} \|\xi\|^{2r} |\hat{f}(\xi)|^2 d\xi\right)^{\frac{1}{2}} \\
&\leq \left(\int_{Q_0} |\hat{f}(\xi)|^2 \mathcal{E}_\varphi(s, T\xi) d\xi\right)^{\frac{1}{2}} + \left(\frac{Ts}{\pi}\right)^r \left(\sum_{n \neq 0} \frac{1}{\|n\|^{2r}}\right)^{\frac{1}{2}} \|f\|_{W_2^r}.
\end{aligned}$$

Here the sum $\sum_{n \neq 0} \|n\|^{-2r}$ is convergent because $r > d/2$. After recalling that $Q_0 = [-\pi/(Ts), \pi/(Ts)]^d$, the above estimate yields (3.8). \square

Note that the remainder in Theorem 3.3 satisfies $\mathcal{R}_\varphi(f, Ts) \rightarrow 0$ as $Ts \rightarrow 0$. Consequently, for every sequence $(T_N, s_N)_{N \in \mathbb{N}}$ we have $\lim_{N \rightarrow \infty} \|\mathbf{P}_{T_N, s_N}f - f\|_{L^2}^2 = 0$ if $T_N s_N \rightarrow 0$ and

$$\int_{[-\frac{\pi}{T_N s_N}, \frac{\pi}{T_N s_N}]^d} |\hat{f}(\xi)|^2 \underbrace{\left(1 - \frac{|\hat{\varphi}(T_N \xi)|^2}{\sum_{k \in \mathbb{Z}^d} |\hat{\varphi}(T_N \xi + 2k\pi/s_N)|^2}\right)}_{=\mathcal{E}_\varphi(s_N, T_N \xi)} d\xi \rightarrow 0.$$

By Lebesgue's dominated convergence theorem this holds if $\mathcal{E}_\varphi(s_N, T_N \xi)$ almost everywhere converges to 0 as $N \rightarrow \infty$. In the following theorem we consider two possible sequences

where this is the case. Note that Item (a) in that theorem is well known (see, for example, [38]), while Item (b) to the best of our knowledge is new.

Theorem 3.4 (Asymptotic behavior of \mathcal{E}_φ). *Let $\varphi \in L^2(\mathbb{R}^d) \cap L^1(\mathbb{R}^d)$.*

(a) *Suppose that $\hat{\varphi}(0) > 0$. Then, for every $s \in (0, \infty)$ we have that $\lim_{T \rightarrow 0} \mathcal{E}_\varphi(s, T\xi) = 0$ almost everywhere if and only if*

$$\frac{1}{\hat{\varphi}(0)} \sum_{m \in \mathbb{Z}^d} \varphi(x - ms) = \frac{(2\pi)^{d/2}}{s^d} \quad \text{for almost every } x \in \mathbb{R}^d. \quad (3.10)$$

Equation (3.10) is called the partition of unity property.

(b) *Suppose $\hat{\varphi}(\xi) = \mathcal{O}(\|\xi\|^{-p})$ as $\|\xi\| \rightarrow \infty$ for some $p > d/2$. Let $(T_N)_{N \in \mathbb{N}}$ and $(s_N)_{N \in \mathbb{N}}$ be bounded sequences in $(0, \infty)$ with $s_N \rightarrow 0$ as $N \rightarrow \infty$. Then*

$$\lim_{N \rightarrow \infty} \mathcal{E}_\varphi(s_N, T_N \xi) = 0 \quad \text{for every } \xi \in \mathbb{R}^d. \quad (3.11)$$

Proof. (a) We have

$$\begin{aligned} & \lim_{T \rightarrow 0} \mathcal{E}_\varphi(s, T\xi) = 0 \text{ for a.e. } \xi \in \mathbb{R}^d \\ \iff & \lim_{T \rightarrow 0} \sum_{k \neq 0} |\hat{\varphi}(T\xi + 2k\pi/s)|^2 = 0 \text{ for a.e. } \xi \in \mathbb{R}^d \\ \iff & \forall k \in \mathbb{Z}^d \setminus \{0\}: \hat{\varphi}(2k\pi/s) = 0 \\ \iff & \forall k \in \mathbb{Z}^d \setminus \{0\}: \int_{\mathbb{R}^d} \varphi(x) e^{i2\pi x \cdot k/s} dx = 0 \\ \iff & \forall k \in \mathbb{Z}^d \setminus \{0\}: \int_{[0, s]^d} \sum_{m \in \mathbb{Z}^d} \varphi(x - ms) e^{i2\pi x \cdot k/s} dx = 0 \\ \iff & \sum_{m \in \mathbb{Z}^d} \varphi(x - ms) = \frac{(2\pi)^{d/2}}{s^d} \hat{\varphi}(0) \text{ for a.e. } x \in \mathbb{R}^d. \end{aligned}$$

(b) As $\hat{\varphi}(\xi) = \mathcal{O}(\|\xi\|^{-p})$ for $\|\xi\| \rightarrow \infty$ there exist constants $R, C > 0$ such that for $\|\xi\| > R$ we have $|\hat{\varphi}(\xi)| \leq C\|\xi\|^{-p}$. Further, for all $\xi \in \mathbb{R}^d$ and $k \neq 0$ we have $\|T_N \xi - 2\pi k/s_N\| \rightarrow \infty$. Therefore it exists $N_0 \in \mathbb{N}$, such that for all $N \geq N_0$ we have $\|T_N \xi - 2\pi k/s_N\| > c$ and $\|T_N \xi\| \leq \frac{1}{2}\|2\pi k/s_N\|$ for $k \neq 0$. Therefore, for all $N \geq N_0$,

$$\begin{aligned} \sum_{k \neq 0} \left| \hat{\varphi}\left(T_N \xi - \frac{2\pi}{s_N} k\right) \right|^2 & \leq C \sum_{k \neq 0} \left\| T_N \xi - \frac{2\pi}{s_N} k \right\|^{-2p} \\ & \leq C \sum_{k \neq 0} \left| \left\| \frac{2\pi}{s_N} k \right\| - \|T_N \xi\| \right|^{-2p} \\ & \leq C \sum_{k \neq 0} \left| \left\| \frac{2\pi}{s_N} k \right\| - \frac{1}{2} \left\| \frac{2\pi}{s_N} k \right\| \right|^{-2p} \end{aligned}$$

$$\leq C \left(\frac{s_N}{\pi}\right)^{2p} \sum_{k \neq 0} \|k\|^{-2p},$$

which implies (3.11). Note that $\sum_{k \neq 0} \|k\|^{-2p}$ is convergent because $p > d/2$. \square

From Theorems 3.3 and 3.4 one concludes that the system of $(\varphi_{T,s}^k)_{k \in \mathbb{Z}^d}$ yields a vanishing approximation error $\min_{u \in \mathcal{V}_{T,s,\varphi}} \|f - u\|_{L^2}^2$ in either of the following cases:

- (a) φ satisfies the partition of unity property, s is fixed and $T \rightarrow 0$;
- (b) $\hat{\varphi}(\xi) = \mathcal{O}(\|\xi\|^{-d/2-\epsilon})$ for $\|\xi\| \rightarrow \infty$, T is bounded and $s \rightarrow 0$.

In both cases one could derive quantitative error estimates. We do not investigate this issue further since our main emphasis is pointing out that allowing s to vary yields asymptotically vanishing approximation error without the partition of unity property. This is relevant since the partition of unity property cannot be satisfied by any radially symmetric compactly supported function.

Below we study two basic examples for generating functions where Theorems 3.3 and 3.4 can be applied. These are pixel (or voxel) basis functions and generalized Kaiser-Bessel functions. We focus on these basis functions since the pixel basis has been the most common choice in early tomographic image reconstruction while generalized Kaiser-Bessel functions are currently considered as the method of choice. Further, also some standard finite element bases satisfy the partition of unit property; compare with Remark 4.1.

3.3 Example: The pixel basis

The pixel basis (also called voxel basis in the case $d > 2$) has been frequently used for image representation in early tomographic image reconstruction (see, for example [13, 23, 25]). It consists of scaled and translated version of the indicator function of the hyper-cube $[-1/2, 1/2]^d$

$$\chi: \mathbb{R}^d \rightarrow \mathbb{R}: x \mapsto \begin{cases} 1 & \text{if } x \in [-1/2, 1/2]^d \\ 0 & \text{otherwise} \end{cases} \quad (3.12)$$

For every $T, s > 0$, the family $(\chi_{T,s}^k)_{k \in \mathbb{Z}^d}$ with $\chi_{T,s}^k(x) = T^{-d/2} \chi((x - Tsk)/T)$ clearly forms a Riesz basis of

$$\mathcal{V}_{T,s,\chi} = \overline{\text{span}\{\chi_{T,s}^k \mid k \in \mathbb{Z}^d\}}.$$

Note that the Fourier transform of χ is given by

$$\hat{\chi}: \mathbb{R} \rightarrow \mathbb{C}: \xi \mapsto (2\pi)^{-d/2} \text{sinc}\left(\frac{\xi}{2}\right) := (2\pi)^{-d/2} \prod_{j=1}^d \text{sinc}\left(\frac{\xi_j}{2}\right), \quad (3.13)$$

where $\text{sinc}(a) := \sin(a)/a$ for $a \neq 0$ and $\text{sinc}(0) := 1$. We see $\hat{\chi}(\xi) = \mathcal{O}(\|\xi\|^{-1})$ as $\|\xi\| \rightarrow \infty$. Consequently, we cannot conclude from Theorem 3.3 that the spaces $\mathcal{V}_{T,s,\chi}$ yields an asymptotically vanishing approximation error for $s \rightarrow 0$.

However, the pixel basis allows to consider the stationary case where s is a constant and where T tends to 0. In fact, from the proof of Theorem 3.4 we see that χ satisfies the partition of unity property if and only if $\text{sinc}(\pi k/s) = 0$ for every $k \neq 0$. This in turn is the case if and only if $s = 2^{-m}$ for some $m \in \mathbb{N}$. The case $s = 1$ seems the most natural one, since it uses non-overlapping basis functions filling the whole space \mathbb{R}^d . The non-overlapping case is in fact used in existing tomographic image reconstruction algorithms; see [13, 23, 25]. Further, note that the number of basis elements $\chi_{T,s}^k$ for which its center $m_k := Tsk$ is contained in the unit cube $[-1, 1]^d$ is given by $(2/(Ts) + 1)^d$ and that T is inversely proportional to the essential bandwidth of the basis function. Therefore, the choice $s = 1$ yields to a minimal number of pixel basis functions representing a function with given support and essential bandwidth.

3.4 Example: Generalized Kaiser-Bessel functions

As often argued in the literature on tomographic image reconstruction, the lack of continuity and rotation invariance are severe drawbacks of the pixel basis functions for image reconstruction. Therefore in [33] the generalized Kaiser-Bessel (KB) functions have been introduced and proposed for image reconstruction.

The generalized KB functions in \mathbb{R}^d form a family of functions that depend on three parameters $m \in \mathbb{N}$, $\gamma \geq 0$ and $a > 0$, where $m \in \mathbb{N}$ is referred to as the order, $\gamma \geq 0$ the taper parameter and $a > 0$ is the support parameter. More precisely, the KB function $\varphi(\cdot; m, \gamma, a): \mathbb{R}^d \rightarrow \mathbb{R}$ of order m is defined by

$$\varphi(x; m, \gamma, a) := \begin{cases} \left(\sqrt{1 - \|x\|^2/a^2} \right)^m \frac{I_m(\gamma \sqrt{1 - \|x\|^2/a^2})}{I_m(\gamma)} & \text{if } \|x\| \leq a \\ 0 & \text{otherwise,} \end{cases} \quad (3.14)$$

where I_m is the modified first kind Bessel function. The window taper γ describes how spiky the basis function is and a is the support radius. The order allows to control the smoothness and the taper parameter allows to further tune the shape of the basis function.

The Fourier transform $\hat{\varphi}(\cdot; m, \gamma, a)$ of the KB function $\varphi(\cdot; m, \gamma, a)$ can be computed to (see [33])

$$\hat{\varphi}(\xi; m, \gamma, a) := \begin{cases} \frac{a^d \gamma^m}{I_m(\gamma)} \frac{I_{d/2+m}(\sqrt{\gamma^2 - a^2 \|\xi\|^2})}{(\sqrt{\gamma^2 - a^2 \|\xi\|^2})^{d/2+m}} & \text{if } a \|\xi\| \leq \gamma \\ \frac{a^d \gamma^m}{I_m(\gamma)} \frac{J_{d/2+m}(\sqrt{a^2 \|\xi\|^2 - \gamma^2})}{(\sqrt{a^2 \|\xi\|^2 - \gamma^2})^{d/2+m}} & \text{otherwise.} \end{cases} \quad (3.15)$$

Here J_m denotes the first kind Bessel function of order m . The known asymptotic decay $J_{d/2+m}(r) = \mathcal{O}(r^{-1/2})$ implies that the asymptotic behavior of the generalized KB function is $\hat{\varphi}(\xi; m, \gamma, a) = \mathcal{O}(\|\xi\|^{-(d/2+m+1/2)})$. From Theorem 3.4 we therefore conclude that for any choice of m , a and γ , the spaces

$$\mathcal{V}_{T,s,\varphi(\cdot; m, \gamma, a)} = \overline{\text{span}\{\varphi_{T,s}^k(\cdot; m, \gamma, a) \mid k \in \mathbb{Z}^d\}}$$

yield vanishing approximation error when $s \rightarrow 0$ and T keeps bounded. Note that the parameter a plays exactly the same roles as the parameter T . Therefore without loss of

generality one could omit a in the definition of the KB functions. However we include it since it is standard to consider the KB functions as a family of three parameters.

Note that the KB function (as any other radially symmetric basis function with compact support) does not satisfy the partition of unity condition. Therefore, Theorem 3.3 implies (for sufficiently regular functions) that the asymptotic approximation error saturates; that is, we have

$$\lim_{T \rightarrow 0} \|\mathbf{P}_{T,s}f - f\|_{L^2}^2 = A_{\varphi,s} \|f\|_{L^2}^2 \quad \text{with} \quad A_{\varphi,s} := \frac{\sum_{k \neq 0} |\hat{\varphi}(2k\pi/s)|^2}{\sum_{k \in \mathbb{Z}^d} |\hat{\varphi}(2k\pi/s)|^2}. \quad (3.16)$$

Keeping $m = 2$, $a = 2$ and $s = 1$ fixed, in [44] it has been proposed to select the taper parameter γ in such a way that the asymptotic approximation error given by $A_{\varphi,s}$ is minimized. Although such a procedure does not overcome the saturation phenomenon, the saturation effect (for given order and given redundancy factor) is minimized. Oppose to that, our theory shows that taking s variable and non-constant overcomes the saturation phenomenon.

In case the partition of unity property does not hold, another natural strategy to address the saturation phenomenon is first considering $T \rightarrow 0$ while keeping s fixed. In a second step one studies the saturation error $A_{\varphi,s}$ defined in (3.16) as $s \rightarrow 0$. Similar to Theorem 3.4 one can show that the saturation error vanishes in limit. More precisely, the following theorem holds.

Theorem 3.5 (Saturation error in the limit). *Let $\varphi \in L^2(\mathbb{R}^d) \cap L^1(\mathbb{R}^d)$ be such that $(\varphi_{T,s}^k)_{k \in \mathbb{Z}^d}$ is a Riesz-basis of $\mathcal{V}_{T,s,\varphi}$ with $\hat{\varphi}(\xi) = \mathcal{O}(\|\xi\|^{-p})$ as $\|\xi\| \rightarrow \infty$ for some $p > d/2$, and let $f \in W_2^r(\mathbb{R}^d)$ with $r > d/2$. Then (3.16) holds and $\lim_{s \rightarrow 0} A_{\varphi,s} = 0$.*

Proof. We have

$$A_{\varphi,s} = \frac{\sum_{k \neq 0} |\hat{\varphi}(2k\pi/s)|^2}{\sum_{k \in \mathbb{Z}^d} |\hat{\varphi}(2k\pi/s)|^2} = 1 - \frac{|\hat{\varphi}(0)|^2}{|\hat{\varphi}(0)|^2 + \sum_{k \neq 0} |\hat{\varphi}(2k\pi/s)|^2}.$$

Therefore the claim follows after showing $\sum_{k \neq 0} |\hat{\varphi}(2k\pi/s)|^2 \rightarrow 0$ as $s \rightarrow 0$. Since $\hat{\varphi}(\xi) = \mathcal{O}(\|\xi\|^{-p})$, there exist $C, s_0 > 0$ with $|\hat{\varphi}(2k\pi/s)| \leq C \|2k\pi/s\|^{-p}$ for $k \neq 0$ and $s \leq s_0$. This implies $\sum_{k \neq 0} |\hat{\varphi}(2k\pi/s)|^2 \leq C (\frac{s}{2\pi})^{2p} \sum_{k \neq 0} \|k\|^{-2p}$. Because $p > d/2$, the sum $\sum_{k \neq 0} \|k\|^{-2p}$ is absolutely convergent. Hence we have $\sum_{k \neq 0} |\hat{\varphi}(2k\pi/s)|^2 \rightarrow 0$ as $s \rightarrow 0$ which concludes the proof. \square

4 The Galerkin approach for PAT using shift invariant spaces

In this section we give details how to efficiently implement the least squares Galerkin method using subspaces of a shift invariant space. This is in contrast to the use of a general reconstruction space, where both the computation of the system matrix and the solution of the Galerkin equation can be slow. For shift invariant spaces the system matrix takes a very special form which allows an efficient implementation.

Let $\varphi \in L^2(\mathbb{R}^d)$ be such that the elements $\varphi_{T,s}^k$ form a Riesz basis of $\mathcal{V}_{T,s,\varphi}$; see Section 3. Moreover, let $(T_N)_{N \in \mathbb{N}}$ and $(s_N)_{N \in \mathbb{N}}$ be two sequences of positive numbers describing the support and the redundancy of the basis functions, respectively. We consider the reconstruction spaces

$$\mathcal{X}_N := \left\{ \sum_{k \in \Lambda_N} c_k \varphi_N^k \mid k \in \Lambda_N \right\} \subseteq \mathcal{V}_{T_N, s_N}, \quad (4.1)$$

where $\varphi_N^k := \varphi_{T_N, s_N}^k$ are the basis functions (with φ_{T_N, s_N}^k as in (3.2)), and $\Lambda_N := \{k \in \mathbb{Z}^d \mid m_k := T_N s_N k \in \overline{B_R(0)}\}$ denotes the set of all $k \in \mathbb{Z}^d$ such that the mid-point m_k of the k -th basis function is contained in $B_R(0)$. Then $\dim \mathcal{X}_N = |\Lambda_N|$ is the number of basis elements used for image representation. In the case that the support of the function to be reconstructed intersects (or is at least close) to $\partial B_R(0)$, it may be better to use all basis functions φ_{T_N, s_N}^k whose support intersects $\overline{B_R(0)}$. The following consideration also hold for such an alternative choice. Further note that the approximation results for the shift invariant spaces $\mathcal{V}_{T,s}$ do not immediately yield approximation results the finite dimensional spaces \mathcal{X}_N . Such investigates are an interesting aspect of future studies.

When applied with the reconstruction space \mathcal{X}_N , our Galerkin approach to PAT analyzed in Section 2 takes the form (see Theorem 2.2)

$$f_N = \sum_{k \in \Lambda_N} c_{N,k} \varphi_N^k, \quad (4.2)$$

where

- $\mathbf{A}_N := (\frac{R}{2} \langle \varphi_N^k, \varphi_N^\ell \rangle_{L^2})_{k, \ell \in \Lambda_N}$ is the system matrix ;
- $d_N := (\langle \mathbf{W} \varphi_N^k, g \rangle_t)_{k \in \Lambda_N}$ is the right hand side;
- $c_N := (c_{N,k})_k$ solves the Galerkin equation $\mathbf{A}_N c_N = d_N$.

As discussed in the following subsection, for the shift invariant case the system matrix \mathbf{A}_N takes a very special form which significantly simplifies the computations. Further, the right hand of the Galerkin equation can be computed efficiently as described in Subsection 4.2 below.

4.1 Evaluation of the system matrix

For any $N \in \mathbb{N}$ and any $k, \ell \in \Lambda_N$, the entries of the system matrix \mathbf{A}_N satisfy

$$\begin{aligned} \langle \varphi_N^k, \varphi_N^\ell \rangle &= \frac{1}{T_N^d} \int_{\mathbb{R}^d} \varphi \left(\frac{x}{T_N} - s_N k \right) \varphi \left(\frac{x}{T_N} - s_N \ell \right) dx \\ &= \int_{\mathbb{R}^d} \varphi(y - s_N k) \varphi(y - s_N \ell) dy \\ &= \int_{\mathbb{R}^d} \varphi(x) \varphi(x - s_N(\ell - k)) dx \\ &= \langle \varphi_{1, s_N}^0, \varphi_{1, s_N}^{\ell - k} \rangle. \end{aligned}$$

Hence instead of computing and storing the whole system matrix required by standard Galerkin methods, in our approach only the values $\langle \varphi_{1,s_N}^0, \varphi_{1,s_N}^n \rangle$ where $n = \ell - k$ with $\ell, k \in \Lambda_N$ have to be computed and stored. The total number of such inner products is bounded by $2^d |\Lambda_N|$. In the case where φ has small support this number is actually much smaller since $\langle \varphi_{1,s_N}^k, \varphi_{1,s_N}^\ell \rangle$ vanishes if the supports of φ_{1,s_N}^k and φ_{1,s_N}^ℓ do not overlap.

In this paper we mainly consider the (non-overlapping) pixel basis (see Subsection 3.3) and the KB functions in two spatial dimensions (see Subsection 3.4). The pixel basis is an orthonormal system and therefore the system matrix is the identity. The KB functions are radially symmetric. In such a situation we compute the entries $\langle \varphi_{1,s_N}^0, \varphi_{1,s_N}^{\ell-k} \rangle$ of the system matrix \mathbf{A}_N approximately as follows. We numerically computed the inner products $\langle \varphi_{1,s_N}^0, \varphi_{1,s_N}^k \rangle_{L^2}$ for all $k \in \mathbb{Z}^2$ with $\|k\|_2 \leq 2a$ using the rectangle rule. For this we discretized the square $[-a, a]^2$ by an equidistant Cartesian grid with $M \times M$ grid points (x_i, y_j) and computed

$$\langle \varphi_{1,s_N}^0, \varphi_{1,s_N}^k \rangle_{L^2} \simeq \frac{(2a)^2}{(M-1)^2} \sum_{i=1}^M \sum_{j=1}^M \varphi_{1,s_N}^0(x_i, y_j) \varphi_{1,s_N}^k(x_i, y_j). \quad (4.3)$$

The resulting system matrix is a tensor product of Toeplitz matrices.

4.2 Evaluation of the right hand side

In the practical application instead of the continuously sampled data $g = \mathbf{W}f$ only discrete data $g(z_i, t_j)_{i,j}$ are known, where $t_j = jT/N_t$ are N_t equidistant time points in the interval $[0, T]$ and z_i are N_{det} points on the measurement surface $\partial B_R(0)$. In our numerical implementation we approximate the right hand side in the Galerkin equation as follows:

$$\langle \mathbf{W}\varphi_N^k, g \rangle_t \simeq \frac{T}{N_t - 1} \sum_{i=1}^{N_{\text{det}}} \sum_{j=1}^{N_t} w_i (\mathbf{W}\varphi_N^k)(z_i, t_j) g(z_i, t_j) t_j. \quad (4.4)$$

Here w_i are appropriate weights accounting for the density of the sampling points. The right hand side in (4.4) may be interpreted as the exact inner product $\langle \mathbf{W}\varphi_N^k, g^\delta \rangle_t$ for some approximate data $g^\delta \simeq g$, which allows application of our convergence and stability result derived in Theorem 3.4.

In some situations (for example for the KB functions and other radially symmetric basis functions in three dimensions), the solution of $\mathbf{W}\varphi_N^k$ is available analytically (see [10, 56]). In our numerical solutions we use the pixel basis and the KB basis functions in two spatial dimensions, where we are not aware of explicit representations for the corresponding solution of the wave equation. In this case we numerically compute $\mathbf{W}\varphi$ using the well known solution formula for the wave equation (1.1),

$$\mathbf{W}f(z, t) = (\partial_t \mathbf{A}_t \mathbf{M}f)(z, t) := \frac{1}{2\pi} \frac{\partial}{\partial t} \int_0^t \int_{S^1} \frac{rf(z+r\omega)}{\sqrt{t^2-r^2}} ds(\omega) dr. \quad (4.5)$$

Here

$$\forall (z, r) \in \partial B_R(0) \times (0, \infty): \quad \mathbf{M}f(z, r) := \frac{1}{2\pi} \int_{S^1} f(z+r\omega) ds(\omega),$$

$$\forall (z, t) \in \partial B_R(0) \times (0, \infty): \quad \mathbf{A}_t g(z, t) := \int_0^t \frac{r g(z, r)}{\sqrt{t^2 - r^2}} dr,$$

denote the spherical means transform of a function $f: \mathbb{R}^2 \rightarrow \mathbb{R}$ with support in $B_R(0)$, and the Abel transform of a function $g: \partial B_R(0) \times (0, \infty) \rightarrow \mathbb{R}$ in the second variable, respectively. The solution formula (4.5) is used to numerically compute $\mathbf{W}\varphi_N^k$ required for evaluating the right hand side of the Galerkin equation as outlined in the following.

- For a symmetric basis function of the form $\varphi(x) = \bar{\varphi}(\|x\|)$ the corresponding solution of the wave equation also is radially symmetric. Hence in order to approximate $\mathbf{W}\varphi_N^k$ we numerically approximate $\mathbf{W}\varphi_{1,s_N}^0((r_n, 0), t_j)$ for N_r equidistant radii $r_n \in [0, 2R]$ and using a numerical approximation of \mathbf{W} by discretizing the spherical Radon transform as well as the Abel transform in (4.5). As a next step, for any basis functions φ_N^k , we approximately compute

$$\mathbf{W}\varphi_N^k(z_i, t_j) = \mathbf{W}\varphi_{1,s_N}^0(\|z_i - k\|, 0), t_j)$$

at any detector points $z_i \in \partial B_R(0)$ and discrete time points t_j by replacing the right hand side with the piecewise linear interpolation in the first argument using the known values $\mathbf{W}\varphi_{1,s_N}^0((r_n, 0), t_j)$.

- In the case of the pixel basis, the spherical means $\mathbf{M}\chi_N^k$ have been computed analytically and evaluated at the discretization points (z_i, t_j) . Subsequently, the wave data $\mathbf{W}\varphi_N^k(z_i, t_j)$ are computed by numerically evaluating the Abel transform in (4.5).

Remark 4.1 (Implementation for finite element bases). *Above we have demonstrated how the Galerkin approach can be implemented efficiently if \mathcal{X}_N is generated by a radially symmetric function. In fact, an efficient implementation of the Galerkin method for PAT can be obtained for an arbitrary generating element. In this case the entries of the system matrix are computed similar to (4.3). Due to the lack of symmetry of the basis functions, the solution formula (4.5) cannot be used to accelerate the computation of $\mathbf{W}\varphi_N^k$; still this would require the separate evaluation (4.5) for each basis function. In the non-radially symmetric case, however, one can exploit again that $\varphi_N^k(x) = \varphi((x - skT)/T)$ are translates of a single function $\varphi_{T,1}^0$. For that purpose, one first numerically computes the solution $p(x, t)$ of the wave equation (1.1) with initial data $\varphi_{T,1}^0$. In a second step one uses interpolation to approximately find $(\mathbf{W}\varphi_N^k)(z_i, t_j) = p(z_i - skT, t_j)$.*

Such an approach can, for example, be used for a bilinear finite elements basis that consists of scaled and translated versions of the basis function $\varphi: \mathbb{R}^2 \rightarrow \mathbb{R}$ defined by

$$\varphi(x) := \begin{cases} (1 - |x_1|)(1 - |x_2|) & (x_1, x_2) \in [-1, 1]^2 \\ 0 & \text{else.} \end{cases} \quad (4.6)$$

The corresponding finite element basis using the shift parameter $s = 1/2$ can easily be seen to satisfy the partition of unity property. Note that in this case the entries of the system matrix even can be computed analytically. Exploring the use of finite elements further is beyond the scope of this paper. However, we think that a precise comparison of different basis elements (in combination with our Galerkin approach as well as in combination with related approaches) is an interesting and important line of future research.

5 Numerical studies

In this section we present results of our numerical studies for our Galerkin least squares approach, where the approximation space \mathcal{X}_N is taken as the subspace of a shift invariant space. We further compare our results with related approaches in the literature. We restrict ourselves to the case of two spatial dimensions and take $R = 1$ for the radius of the measurement circle.

For all presented numerical results, the function f is taken a superposition of indicator functions as shown in top left image in Figure 5.1. The corresponding discrete data

$$g(z_i, t_j) \simeq (\mathbf{W}f)(z_i, t_j) \quad \text{for } i = 1, \dots, N_{\text{det}} \text{ and } j = 1, \dots, N_t, \quad (5.1)$$

where $z_i = (\cos(i2\pi/N_{\text{det}}), \sin(i2\pi/N_{\text{det}}))$ denote the equidistant detector locations and $t_j = jT/N_t$ the discrete time points, have been computed numerically by implementing (4.5). For that purpose we discretized the spherical Radon transform as well as the Abel transform in (4.5). We take $T = 3$ as the final measurement time, $N_{\text{det}} = 100$, $N_t = 376$ for the discretization of the data and $N_x = 300$ for discretizing the function. Note that the data are computed in a way that is completely different from the Galerkin system which avoids any inverse crime.

5.1 Reconstruction results using Kaiser-Bessel Functions

We first investigate the case where $\varphi = \varphi(\cdot; m, a, \gamma)$ is a KB function. The parameters m and γ determine the shape and smoothness of the KB function, whereas a determines its support. It is therefore reasonable to fix m and γ . Here we choose the fixed parameters $m = 1$ and $\gamma = 2$. Further, a determines the support of the KB function, which is also controlled by the parameter T . Therefore also this parameter can be fixed; without loss of generality we take $a = 2$. This effects that for $s = 1$ the functions φ_N^k show sufficient overlap. Since the total number of basis functions which are centered in the square $[-1, 1]^2$ is equal to N^2 with $N = 2/(sT) + 1$ it is reasonable to consider combinations of the parameters s and T where the product sT remains constant.

The proposed KB Galerkin approach for the inverse PAT problem consists in solving the Galerkin equation (4.2). Therefore the system matrix and the right hand side are computed in MATLAB as described in Section 4 and the direct solver `mldivide` is used for numerically computing the solution of (4.2). Figure 5.1 shows reconstructions using the KB Galerkin reconstruction for $N = 100$ and step size parameters $s = 0.8081$, $s = 1.0101$ and $s = 1.3636$, respectively. One notices that actually all considered step size parameters yield quite good results.

5.2 Parameter selection for the KB functions

Choosing optimal parameters seems a difficult issue. In the following we numerically investigate the optimal choice of the parameters s and T for a fixed number of basis functions N^2 with $N = 50$ and $N = 100$, respectively. For that purpose we compute the L^2 -reconstruction

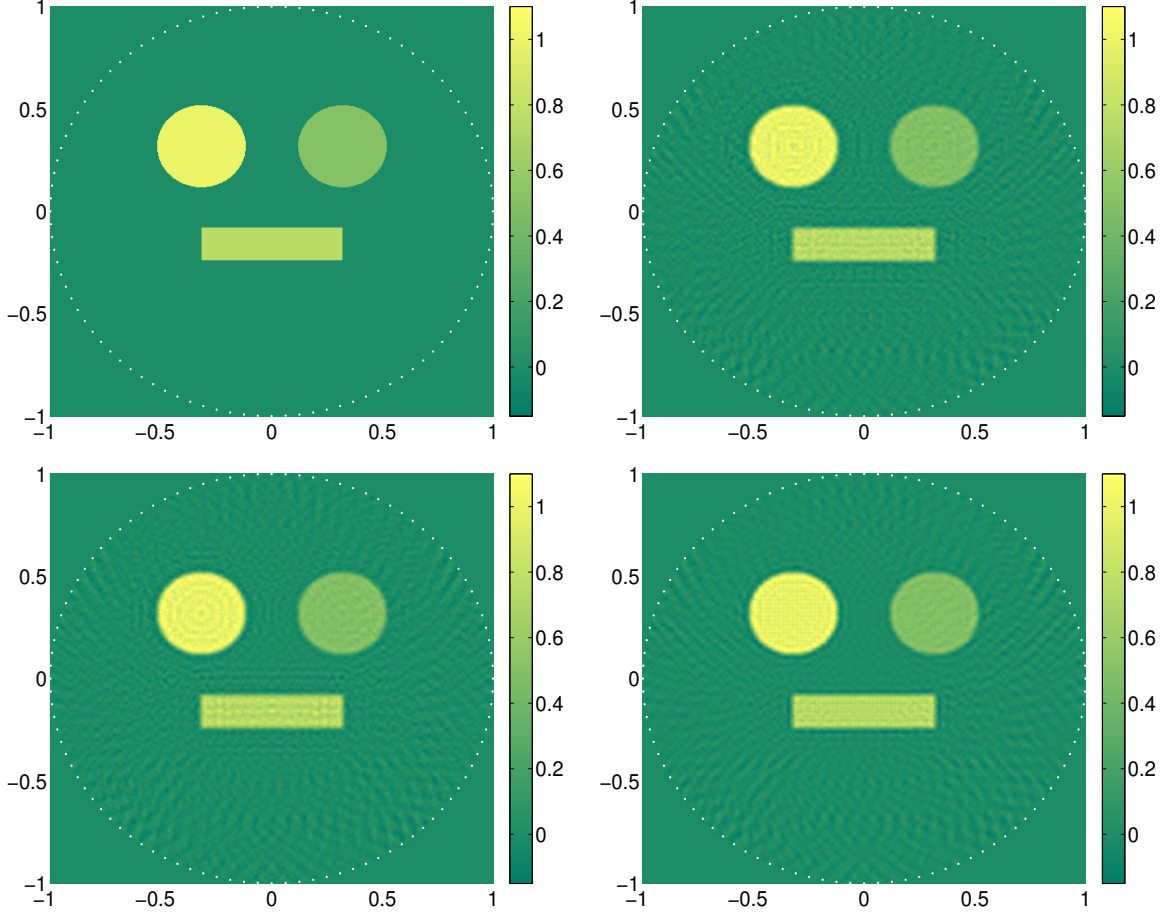


Figure 5.1: RECONSTRUCTION RESULTS USING THE PROPOSED KB GALERKIN APPROACH. Top left: Phantom f . Top right: Reconstruction with $s = 0.8081$, $T = 0.025$. Bottom left: Reconstruction with $s = 1.0101$, $T = 0.02$. Bottom right: Reconstruction with $s = 1.3636$ and $T = 0.0148$.

error

$$e_N(s, f) := \frac{\sum_{i=1}^N \sum_{j=1}^N |f_N(x_i, y_j) - f(x_i, y_j)|^2}{\sum_{i=1}^N \sum_{j=1}^N |f(x_i, y_j)|^2}. \quad (5.2)$$

for different choices of s and T satisfying the side condition $sT = 2/(N - 1)$. Here $f_N := \sum_{k \in \Lambda_N} c_{N,k} \varphi_N^k$ is the Galerkin reconstruction given by (4.2) and the evaluation points (x_i, y_j) for evaluating the error in (5.2) are taken as the elements on $\{s_N T_N k \mid k \in \mathbb{Z}^2\} \cap [-1, 1]^2$. In Table 5.1 we show these relative L^2 reconstruction errors. From Table 5.1 one finds that for the considered function optimal choices for the step size parameter are $s = 1.3265$ for $N = 50$ and $s = 1.3131$ for $N = 100$.

From Table 5.1 one notices an irregular behavior of the reconstruction error in dependence on s and N . To better understand this issue recall that for a given basis function $\varphi = \varphi(\cdot; m, a, \gamma)$ the best the L^2 -approximation error using functions $\varphi_{T,s}^k$ is given by (see

$N = 50$			$N = 100$		
s	T	$e_N(s, f)$	s	T	$e_N(s, f)$
1.4286	0.0286	0.0412	1.4141	0.0143	0.0336
1.3776	0.0296	0.0379	1.3636	0.0148	0.0299
1.3265	0.0308	0.0351	1.3131	0.0154	0.0298
1.2755	0.0320	0.0352	1.2626	0.0160	0.0303
1.2245	0.0333	0.0369	1.2121	0.0167	0.0307
1.1735	0.0348	0.0401	1.1616	0.0174	0.0320
1.1224	0.0364	0.0439	1.1111	0.0182	0.0345
1.0714	0.0381	0.0427	1.0606	0.0190	0.0367
1.0204	0.0400	0.0428	1.0101	0.0200	0.0384
0.9694	0.0421	0.0403	0.9596	0.0211	0.0335
0.9184	0.0444	0.0391	0.9091	0.0222	0.0392
0.8673	0.0471	0.0412	0.8586	0.0235	0.0366
0.8163	0.0500	0.0432	0.8081	0.0250	0.0322
0.7653	0.0533	0.0464	0.7576	0.0267	0.0365

Table 5.1: RELATIVE L^2 -RECONSTRUCTION ERRORS For different choices of s the reconstruction error $e_N(s, f)$ with is evaluated for $N = 50$ and $N = 100$. Recall that s is the step size and $T = 2/(s(N - 1))$ determines the size of the KB basis functions.

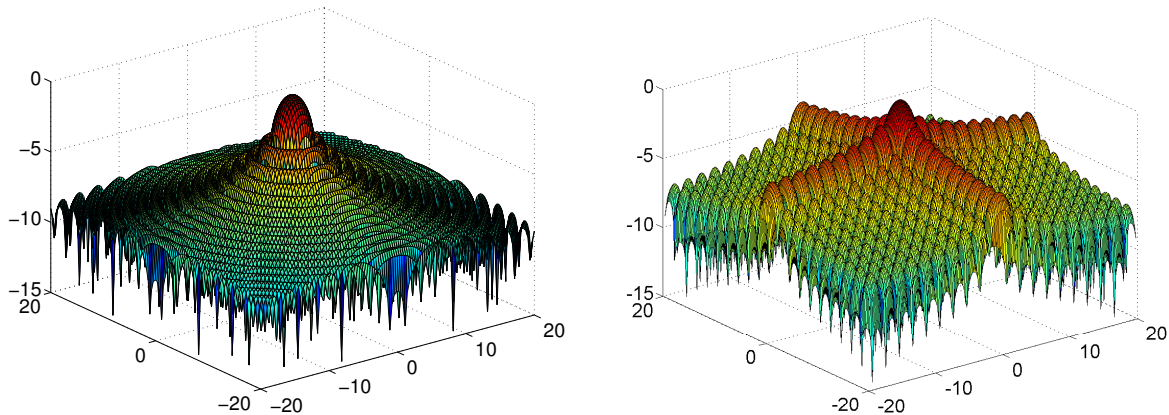


Figure 5.2: LOGARITHMIC PLOTS OF THE FOURIER TRANSFORMS OF THE BASIS FUNCTIONS. Left: Fourier transform $\log(|\hat{\varphi}(\cdot; 1, 2, 2)|)$ of the KB basis function. Right: Fourier transform $\log(|\text{sinc}(\cdot)|)$ of the pixel basis function χ .

Theorem 3.3)

$$\|\mathbf{P}_{T,s}f - f\|_{L^2} = \int_{[-\frac{\pi}{Ts}, \frac{\pi}{Ts}]} |\hat{f}(\xi)|^2 \left(1 - \frac{|\hat{\varphi}(T\xi)|^2}{\sum_{k \in \mathbb{Z}^d} |\hat{\varphi}(T\xi + 2k\pi/s)|^2}\right),$$

where it is assumed that the Fourier transform of f is sufficiently small outside $[-\pi/(Ts), \pi/(Ts)]^2$. Hence for fixed N a “good” choice of s should be made at least in such a way that

$$S_\varphi(s, N, \xi) := \frac{\sum_{k \neq 0} |\hat{\varphi}(\frac{2}{s(N-1)}\xi - \frac{2k\pi}{s})|^2}{|\hat{\varphi}(\frac{2}{s(N-1)}\xi)|^2} \text{ is “small” for } \|\xi\| \leq \frac{\pi(N-1)}{2}.$$

(We have taken $T = 2/(s(N-1))$ and \hat{f} is supposed to be unknown.) Figure 5.2 shows that absolute value of the radially symmetric Fourier transform of the basis function $\varphi(\cdot; 1, 2, 2)$ in a logarithmic plot. This shows a complicated dependence of $S_\varphi(s, N, \xi)$ on s , N and ξ and indicates that a simple universally valid answer how to optimally chose parameters seems difficult. We further note that $S_\varphi(s, N, \xi)$ does not contain error due to frequency content outside $[-\pi/(Ts), \pi/(Ts)]^2$. Nevertheless, theoretical error estimates in combination with numerical studies can give precise guidelines for selecting good parameter for the practical applications. The quality of the reconstruction depends on the parameters of the KB function m, γ, a as well as on s and T (note that T has a similar role as a). In the paper [44] the authors studied optimizing the parameter γ (in the limit $T \rightarrow 0$) while the parameters $s = 1$, $a = 2$ and $m = 2$ have been kept fixed. For that purpose they choose the parameter γ in $\varphi(\cdot; 2, 2, \gamma)$ such that the limiting residual error $S_\varphi(1, 0, \xi) = \sum_{k \neq 0} |\hat{\varphi}(2k\pi)|^2$ (that is independent of ξ) becomes minimal. As we argued above the drawback of such an approach is that taking s fixed does not yield vanishing asymptotic error as $N \rightarrow \infty$. Allowing s to depend on N overcomes this issue but makes the parameter selection more complicated.

5.3 Comparison with state of the art reconstruction methods

We compare our Galerkin approach using KB functions with other state of the art approaches for PAT image reconstruction. We used the same phantom as above and the same wave data $\mathbf{W}f$ for all reconstruction methods. We selected 100×100 basis functions. For the KB Galerkin approach we use the generating function $\varphi(\cdot; 1, 2, 2)$ with step size parameter $s = 0.8081$ and correspondingly $T = 0.025$.

The KB Galerkin-least squares approach is compared to the following methods:

- **Discrete-discrete KB imaging model [56].** We compare our method also to the DD (discrete-discrete) image reconstruction approach using KB functions proposed in [56]. There the same basis functions for approximating the unknown function are used, $f_N = \sum_{k \in \Lambda_N} c_{N,k} \varphi_N^k$. Opposed to our Galerkin approach, for recovering the coefficients in the basis expansion one forces $\mathbf{W}f_N$ to exactly interpolate the discrete data values $g(x_i, t_j)$. This is equivalently characterized as the minimizer of following discrete data least squares functional over \mathcal{X}_N ,

$$\frac{1}{2} \|\mathbf{B}_N c_N - g_N\|^2 \rightarrow \min_{c_N} \quad (5.3)$$

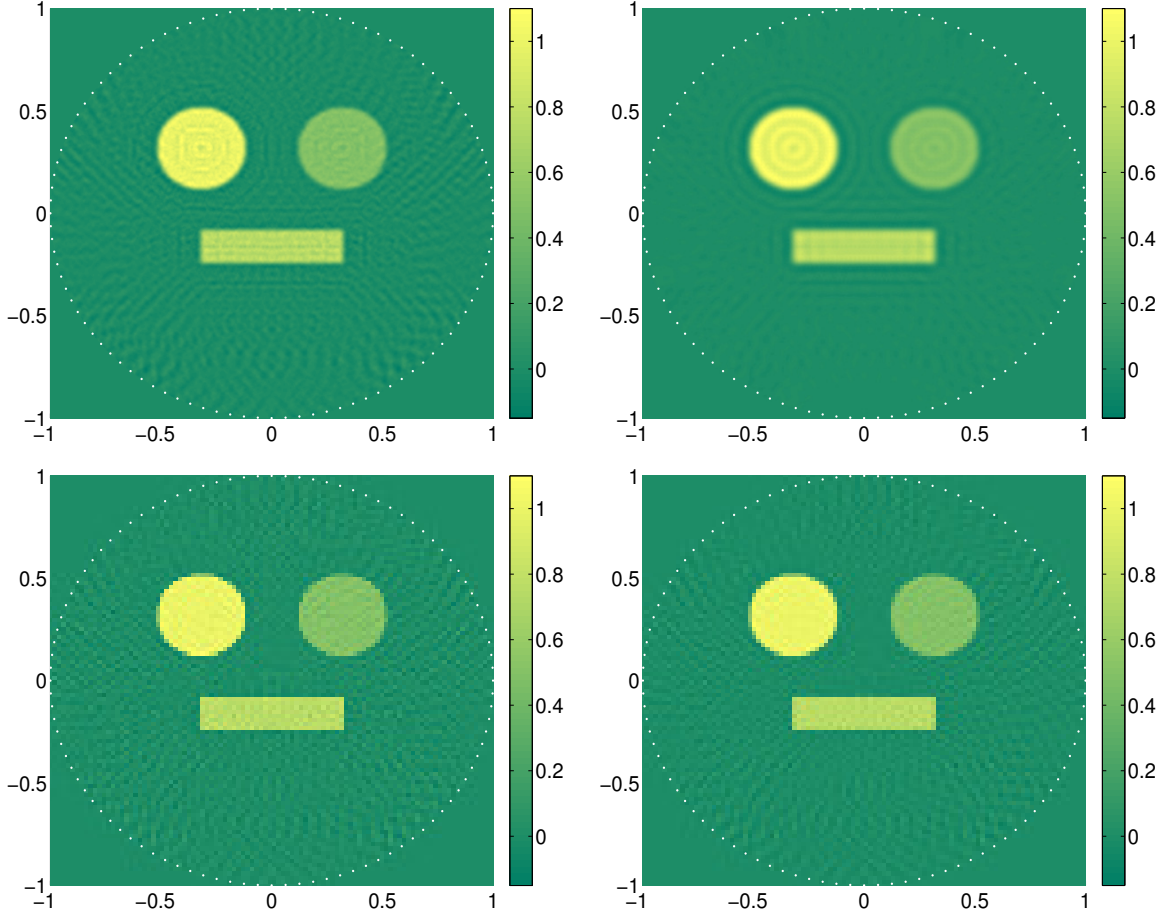


Figure 5.3: COMPARISON OF RECONSTRUCTION METHODS. Top left: KB Galerkin approach using 40 CG iterations. Top right: Fully discrete KB reconstruction using 40 CG iterations. Bottom left: FBP algorithm. Bottom right: Galerkin reconstruction using pixel basis.

where $\mathbf{B}_N := (\mathbf{W}\varphi_N^k(x_i, t_j))_{i,k}$ and $g_N := (g(x_i, t_j))_{i,j}$. Note that in [56] it has been proposed to add an additional regularization term to (5.3), which we do not consider here.

- **Filtered backprojection (FBP) algorithm.** For the filtered backprojection algorithm we implemented the explicit inversion formula

$$\begin{aligned}
 f(x) &= \frac{2}{R} (\mathbf{W}^* t \mathbf{W} f)(x) \\
 &= -\frac{1}{\pi} \int_{\partial D_1} \int_{|x-p|}^{\infty} \frac{\partial_t (t \mathbf{W} f(p, t))}{\sqrt{t^2 - |x-p|^2}} dt ds(p) \quad \text{for all } x \in B_R(0). \quad (5.4)
 \end{aligned}$$

The inversion formula has been derived in [12] for odd spatial dimension and in [11] for even dimension. The inversion formula (5.4) can be efficiently implemented in the form of a filtered backprojection algorithm requiring $\mathcal{O}(N^3)$ floating operations, where $N \times N$ is the number of reconstruction points, see [7, 11]. For a fair comparison, the

number of reconstruction points in the filtered backprojection algorithm is taken equal to the number of basis functions in the KB Galerkin approach.

■ **Galerkin reconstruction using the pixel basis.**

Here reconstruction space is generated by 100×100 basis functions given by piecewise constant functions on a square of length $2/100$ (see Section 3.3). Since the pixel basis forms an orthonormal system it holds $\mathbf{A}_N = \mathbf{I}_N$. The right hand side of the matrix equation is computed as described in Section 4.

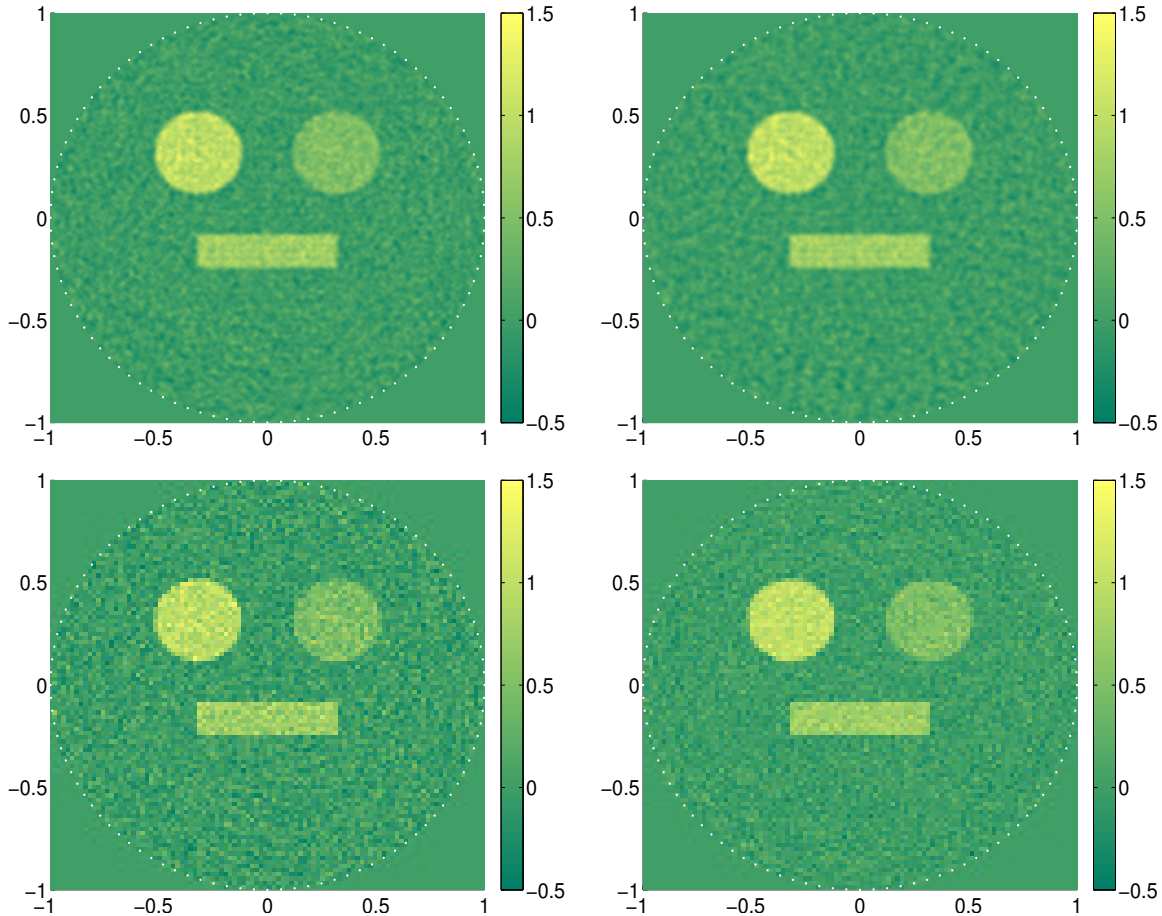


Figure 5.4: COMPARISON OF RECONSTRUCTION METHODS FOR DATA WITH 5% NOISE. Top left: KB Galerkin approach using 40 CG iterations. Top right: Fully discrete KB reconstruction using 40 CG iterations. Bottom left: FBP algorithm. Bottom right: Galerkin reconstruction using pixel basis.

The minimizer of the optimization problem (5.3) is given as the solution of the normal equation $\mathbf{B}_N^T \mathbf{B}_N c = \mathbf{B}_N^T g_N$. The matrix $\mathbf{B}_N^T \mathbf{B}_N$ is less structured and less sparse than our Galerkin matrix \mathbf{A}_N . We observed that the direct solver in MATLAB was much slower than for the Galerkin method (more than a minute compared to a fraction of a second) and therefore we decided to use iterative methods for its solution. In particular we found

the CG algorithm to perform good, which has been used for the results shown below. For better comparison we also computed the KB Galerkin solution using the CG method. Iteratively addressing the arising equations has the advantage that they are applicable for three dimension image reconstruction as well.

In Figure 5.3 we show reconstruction results with the above methods applied to the simulated data obtained on a standard desktop PC. Computing the right hand side in the Galerkin equation took about 1.95 seconds for the KB functions and 2.04 for the pixel basis. The solution of the KB Galerkin equation took 0.31 seconds with the direct MATLAB solver and 0.11 seconds using 40 steps of the CG equation. The solution of the discrete equation took about 76.17 seconds with the direct MATLAB solver and 5.01 seconds using 40 steps of the CG equation. The used filtered backprojection algorithm took about 0.08 seconds. One observes that computing the right hand side is currently the most time consuming part in the Galerkin approach. Since we have to compute N^2 inner products and each inner product consist of a sum over $N_{\text{det}}N_t$ components, the numerical effort of that step is $\mathcal{O}(N^4)$ if we take $N_{\text{det}} = \mathcal{O}(N)$ and $N_t = \mathcal{O}(N)$. By exploiting the special structure of the basis functions and the wave operator we believe that it might be possible to derive $\mathcal{O}(N^3)$ algorithm for evaluating the right hand side. In such a situation we would reach the computational performance of the FPB algorithm with more flexibility and a potentially better accuracy. Further note that the matrix $\mathbf{B}_N^T \mathbf{B}_N$ in the DD approach is not sparse which explains why the CG method for the Galerkin approach is faster than the CG method for the DD approach. In three spatial dimension, both the DD approach (see [56]) and the Galerkin approach yields to a sparse system matrix and therefore both have similar and good numerical efficiency in this case.

In order to investigate the stability of the above algorithms with respect to noise we repeated the above computation after Gaussian white noise with variance equal to 5% of the L^2 -norm of the data. The results are shown in Figure 5.4. Table 5.2 summarizes the L^2 -reconstruction for different noise level and different reconstruction errors. We see that the methods using the KB functions perform best in terms of the L^2 -reconstruction error. Note that the early stopping of the CG methods has a regularization effect. This partially explains the smaller reconstruction error of the method using the CG iteration. We emphasize that we did not select the number of iterations to minimize the reconstruction error. The KB Galerkin using the direct solver in MATLAB also gives quite small error, which indicates that early stopping is not a very important issue in terms of the stability. Note that for noisy data all results can be improved by incorporating regularization (see, for example, [14] for the FBP algorithm and [56] for the DD approach).

6 Conclusion and outlook

In this paper we studied (least-squares) Galerkin methods for photoacoustic tomography with spherical geometry (and arbitrary dimension). We implemented our Galerkin approach for two spatial dimensional and presented numerical results demonstrating that yields accurate results. The considered approach yields to solution of the Galerkin equation $\mathbf{A}_N \mathbf{c}_N = \mathbf{b}_N$, where the system matrix \mathbf{A}_N has size $N^2 \times N^2$ with N^2 denoting the number of basis elements.

noise (%)	Galerkin	Galerkin (CG)	DD approach (CG)	FBP	Pixel
0	0.0323	0.0306	0.0314	0.0347	0.0283
2.5	0.0830	0.0748	0.0783	0.2064	0.1249
5	0.1411	0.1272	0.1140	0.3897	0.2092

Table 5.2: RELATIVE L^2 -RECONSTRUCTION ERRORS FOR $N = 100$, $s = 0.8081$ USING DIFFERENT RECONSTRUCTION METHODS AND DIFFERENT NOISE LEVELS. The Galerkin, the Galerkin (CG) and DD-approach (CG) we use the the KB basis function $\varphi(\cdot; 1, 2, 2)$. For the methods using the CG algorithm 40 iterative steps have been performed.

For a general reconstruction space, the system matrix to be computed and stored is dense and unstructured. In this paper we showed that by using the isometry property of [11, 12] in combination with translation invariant reconstruction spaces, the system matrix is sparse and has simple structure. This can be used to easily set up the Galerkin equation and efficiently solve the Galerkin equation. This is in contrast to existing model based approaches for two-dimensional PAT, that do not yield to a sparse system matrix and numerical solvers for the arising equation (such as the CG algorithm) are numerically more expensive.

There are several possible interesting extensions and modifications of our image reconstruction approach. One intended line of research is the extension of our algorithm to three spatial dimension. For that purpose we believe that it is most promising to use iterative methods (such as the CG algorithm) for solving the Galerkin equation. One advantage in this case is that the system matrix is not required to be explicitly stored. For that purpose we will further derive more efficient ways how to evaluate the right hand side in the Galerkin equation which is, at least for the presented algorithm in two spatial dimensions, the most time consuming part. Another practically important extension of our framework is to incorporate finite detector size, finite bandwidth of the detection system and allowing incomplete data. In such cases it will be necessary to include additional regularization to stabilize the reconstruction process. We intend to apply our algorithm to experimental data and to study the optimal parameter choices in such a situation. Finally it would be interesting to extend our approach to more general measurement surfaces.

Acknowledgement

The authors thank the reviewers for careful reading and helpful comments on the manuscript.

References

- [1] M. AGRANOVSKY AND P. KUCHMENT, *Uniqueness of reconstruction and an inversion procedure for thermoacoustic and photoacoustic tomography with variable sound speed*, Inverse Probl., 23 (2007), pp. 2089–2102.

- [2] M. ANSORG, F. FILBIR, W. R. MADYCH, AND R. SEYFRIED, *Summability kernels for circular and spherical mean data*, *Inverse Probl.*, 29 (2013), p. 015002.
- [3] S. R. ARRIDGE, M. M. BETCKE, B. T. COX, F. LUCKA, AND B. E. TREEBY, *On the adjoint operator in photoacoustic tomography*, *Inverse Probl.*, 32 (2016), p. 115012 (19pp).
- [4] P. BEARD, *Biomedical photoacoustic imaging*, *Interface focus*, 1 (2011), pp. 602–631.
- [5] Z. BELHACHMI, T. GLATZ, AND O. SCHERZER, *A direct method for photoacoustic tomography with inhomogeneous sound speed*, *Inverse Probl.*, 32 (2016), p. 045005.
- [6] T. BLU AND M. UNSER, *Approximation error for quasi-interpolators and (multi-)wavelet expansions*, *Appl. Comput. Harmon. Anal.*, 6 (1999), pp. 219–251.
- [7] P. BURGHOLZER, J. BAUER-MARSCHALLINGER, H. GRÜN, M. HALTMEIER, AND G. PALTAUF, *Temporal back-projection algorithms for photoacoustic tomography with integrating line detectors*, *Inverse Probl.*, 23 (2007), pp. S65–S80.
- [8] P. BURGHOLZER, G. J. MATT, M. HALTMEIER, AND G. PALTAUF, *Exact and approximate imaging methods for photoacoustic tomography using an arbitrary detection surface*, *Phys. Rev. E*, 75 (2007), p. 046706.
- [9] X. L. DEAN-BEN, A. BUEHLER, V. NTZIACHRISTOS, AND D. RAZANSKY, *Accurate model-based reconstruction algorithm for three-dimensional photoacoustic tomography*, *IEEE Trans. Med. Imag.*, 31 (2012), pp. 1922–1928.
- [10] G. J. DIEBOLD, T. SUN, AND M. I. KHAN, *Photoacoustic monopole radiation in one, two, and three dimensions*, *Phys. Rev. Lett.*, 67 (1991), p. 3384.
- [11] D. FINCH, M. HALTMEIER, AND RAKESH, *Inversion of spherical means and the wave equation in even dimensions*, *SIAM J. Appl. Math.*, 68 (2007), pp. 392–412.
- [12] D. FINCH, S. K. PATCH, AND RAKESH, *Determining a function from its mean values over a family of spheres*, *SIAM J. Math. Anal.*, 35 (2004), pp. 1213–1240.
- [13] R. GORDON, R. BENDER, AND G. T. HERMAN, *Algebraic reconstruction techniques (ART) for three-dimensional electron microscopy and x-ray photography*, *Journal Theor. Biol.*, 29 (1970), pp. 471–481.
- [14] M. HALTMEIER, *A mollification approach for inverting the spherical mean Radon transform*, *SIAM J. Appl. Math.*, 71 (2011), pp. 1637–1652.
- [15] M. HALTMEIER, *Inversion of circular means and the wave equation on convex planar domains*, *Comput. Math. Appl.*, 65 (2013), pp. 1025–1036.
- [16] M. HALTMEIER, *Universal inversion formulas for recovering a function from spherical means*, *SIAM J. Math. Anal.*, 46 (2014), pp. 214–232.

- [17] M. HALTMEIER AND L. V. NGUYEN, *Iterative methods for photoacoustic tomography with variable sound speed*. arXiv:1611.07563, 2016.
- [18] M. HALTMEIER AND S. PEREVERZYEV JR., *Recovering a function from circular means or wave data on the boundary of parabolic domains*, SIAM J. Imaging Sci., 8 (2015), pp. 592–610.
- [19] M. HALTMEIER AND S. PEREVERZYEV JR., *The universal back-projection formula for spherical means and the wave equation on certain quadric hypersurfaces*, J. Math. Anal. Appl., 429 (2015), pp. 366–382.
- [20] M. HALTMEIER, O. SCHERZER, P. BURGHOLZER, R. NUSTER, AND G. PALTAUF, *Thermoacoustic tomography and the circular Radon transform: exact inversion formula*, Math. Mod. Meth. Appl. Sci., 17 (2007), pp. 635–655.
- [21] M. HALTMEIER, T. SCHUSTER, AND O. SCHERZER, *Filtered backprojection for thermoacoustic computed tomography in spherical geometry*, Math. Meth. Appl. Sci., 28 (2005), pp. 1919–1937.
- [22] M. HALTMEIER AND G. ZANGERL, *Spatial resolution in photoacoustic tomography: Effects of detector size and detector bandwidth*, Inverse Probl., 26 (2010), p. 125002.
- [23] G. T. HERMAN, *Basis functions in image reconstruction from projections: A tutorial introduction*, Sens. and Imaging, 16 (2015), pp. 1–21.
- [24] Y. HRISTOVA, P. KUCHMENT, AND L. NGUYEN, *Reconstruction and time reversal in thermoacoustic tomography in acoustically homogeneous and inhomogeneous media*, Inverse Probl., 24 (2008), p. 055006 (25pp).
- [25] A. C. KAK AND M. SLANEY, *Principles of Computerized Tomographic Imaging*, vol. 33 of Classics in Applied Mathematics, Society for Industrial and Applied Mathematics (SIAM), Philadelphia, PA, 2001.
- [26] R. KRESS, *Linear Integral Equations*, Springer Verlag, Berlin, 1999. second edition.
- [27] R. A. KRUGER, W. L. KISER, D. R. REINECKE, G. A. KRUGER, AND K. D. MILLER, *Thermoacoustic molecular imaging of small animals*, Mol. Imaging, 2 (2003), pp. 113–123.
- [28] P. KUCHMENT, *The Radon transform and medical imaging*, SIAM, Philadelphia, 2014.
- [29] P. KUCHMENT AND L. KUNYANSKY, *Mathematics of photoacoustic and thermoacoustic tomography*, in Handbook of Mathematical Methods in Imaging, Springer, 2011, pp. 817–865.
- [30] L. A. KUNYANSKY, *Explicit inversion formulae for the spherical mean Radon transform*, Inverse Probl., 23 (2007), pp. 373–383.

- [31] L. A. KUNYANSKY, *A series solution and a fast algorithm for the inversion of the spherical mean Radon transform*, *Inverse Probl.*, 23 (2007), pp. S11–S20.
- [32] L. A. KUNYANSKY, *Inversion of the spherical means transform in corner-like domains by reduction to the classical Radon transform*, *Inverse Probl.*, 31 (2015).
- [33] R. M. LEWITT, *Multidimensional digital image representations using generalized kaiser–bessel window functions*, *J. Opt. Soc. Am. A*, 7 (1990), pp. 1834–1846.
- [34] R. M. LEWITT, *Alternatives to voxels for image representation in iterative reconstruction algorithms*, *Phys. Med. Biol.*, 37 (1992), p. 705.
- [35] A. K. LOUIS, *Approximate inverse for linear and some nonlinear problems*, *Inverse Probl.*, 12 (1996), pp. 175–190.
- [36] A. K. LOUIS AND P. MAASS, *A mollifier method for linear operator equations of the first kind*, *Inverse Probl.*, 6 (1990), pp. 427–440.
- [37] A. K. LOUIS AND T. SCHUSTER, *A novel filter design technique in 2D computerized tomography*, *Inverse Probl.*, 12 (1996), pp. 685–696.
- [38] S. MALLAT, *A wavelet tour of signal processing: The sparse way*, Elsevier/Academic Press, Amsterdam, third ed., 2009.
- [39] S. MATEJ AND R. M. LEWITT, *Practical considerations for 3-d image reconstruction using spherically symmetric volume elements*, *IEEE Trans. Med. Imag.*, 15 (1996), pp. 68–78.
- [40] F. NATTERER, *The Mathematics of Computerized Tomography*, vol. 32 of Classics in Applied Mathematics, SIAM, Philadelphia, 2001.
- [41] F. NATTERER, *Photo-acoustic inversion in convex domains*, *Inverse Probl. Imaging*, 6 (2012), pp. 315–320.
- [42] L. V. NGUYEN, *A family of inversion formulas for thermoacoustic tomography*, *Inverse Probl.*, 3 (2009), pp. 649–675.
- [43] L. V. NGUYEN AND L. A. KUNYANSKY, *A dissipative time reversal technique for photoacoustic tomography in a cavity*, *SIAM J. Imaging Sci.*, 9 (2016), pp. 748–769.
- [44] M. NILCHIAN, J. P. WARD, C. VONESCH, AND M. UNSER, *Optimized kaiser–bessel window functions for computed tomography*, *IEEE Trans. Image Process.*, 24 (2015), pp. 3826–3833.
- [45] V. NTZIACHRISTOS, J. RIPOLL, L. V. WANG, AND R. WEISSLEDER, *Looking and listening to light: the evolution of whole-body photonic imaging*, *Nat. Biotechnol.*, 23 (2005), pp. 313–320.

- [46] V. P. PALAMODOV, *A uniform reconstruction formula in integral geometry*, Inverse Probl., 28 (2012), p. 065014.
- [47] G. PALTAUF, R. NUSTER, M. HALTMEIER, AND P. BURGHOLZER, *Experimental evaluation of reconstruction algorithms for limited view photoacoustic tomography with line detectors*, Inverse Probl., 23 (2007), pp. S81–S94.
- [48] G. PALTAUF, J. A. VIATOR, S. A. PRAHL, AND S. L. JACQUES, *Iterative reconstruction algorithm for optoacoustic imaging*, J. Opt. Soc. Am., 112 (2002), pp. 1536–1544.
- [49] A. RIEDER AND T. SCHUSTER, *The approximate inverse in action with an application to computerized tomography*, SIAM J. Num. Anal., 37 (2000), pp. 1909–1929.
- [50] A. RIEDER AND T. SCHUSTER, *The approximate inverse in action III: 3D-Doppler tomography*, Num. Math., 97 (2004), pp. 353–378.
- [51] H. ROITNER, M. HALTMEIER, R. NUSTER, D. P. O’LEARY, T. BERER, G. PALTAUF, H. GRÜN, AND P. BURGHOLZER, *Deblurring algorithms accounting for the finite detector size in photoacoustic tomography*, J. Biomed. Opt., 19 (2014), p. 056011.
- [52] A. ROSENTHAL, V. NTZIACHRISTOS, AND D. RAZANSKY, *Acoustic inversion in optoacoustic tomography: A review*, Curr. Med. Imaging Rev., 9 (2013), p. 318.
- [53] Y. SALMAN, *An inversion formula for the spherical mean transform with data on an ellipsoid in two and three dimensions*, J. Math. Anal. Appl., 420 (2014), pp. 612–620.
- [54] B. E. TREEBY AND B. T. COX, *k-wave: Matlab toolbox for the simulation and reconstruction of photoacoustic wave-fields*, J. Biomed. Opt., 15 (2010), p. 021314.
- [55] K. WANG, S. A. ERMILOV, R. SU, H. BRECHT, A. A. ORAEVSKY, AND M. A. ANASTASIO, *An imaging model incorporating ultrasonic transducer properties for three-dimensional optoacoustic tomography*, IEEE Trans. Med. Imag., 30 (2011), pp. 203–214.
- [56] K. WANG, R. W. SCHOONOVER, R. SU, A. ORAEVSKY, AND M. A. ANASTASIO, *Discrete imaging models for three-dimensional optoacoustic tomography using radially symmetric expansion functions*, IEEE Trans. Med. Imag., 33 (2014), pp. 1180–1193.
- [57] K. WANG, R. SU, A. A. ORAEVSKY, AND M. A. ANASTASIO, *Investigation of iterative image reconstruction in three-dimensional optoacoustic tomography*, Phys. Med. Biol., 57 (2012), p. 5399.
- [58] L. V. WANG AND S. HU, *Photoacoustic tomography: in vivo imaging from organelles to organs*, Science, 335 (2012), pp. 1458–1462.
- [59] M. XU AND L. V. WANG, *Time-domain reconstruction for thermoacoustic tomography in a spherical geometry*, IEEE Trans. Med. Imag., 21 (2002), pp. 814–822.

- [60] M. XU AND L. V. WANG, *Analytic explanation of spatial resolution related to bandwidth and detector aperture size in thermoacoustic or photoacoustic reconstruction*, Phys. Rev. E, 67 (2003), pp. 0566051–05660515 (electronic).
- [61] M. XU AND L. V. WANG, *Universal back-projection algorithm for photoacoustic computed tomography*, Phys. Rev. E, 71 (2005), p. 016706.
- [62] J. ZHANG, M. A. ANASTASIO, P. J. LA RIVIÈRE, AND L. V. WANG, *Effects of different imaging models on least-squares image reconstruction accuracy in photoacoustic tomography*, IEEE Trans. Med. Imag., 28 (2009), pp. 1781–1790.